To the Graduate Council:

I am submitting herewith a thesis written by Wesley E. Bryan entitled "Design of Compact Loop Antennas for Present and Future Fusion Heating Experiments." I have examined the final copy of this thesis for form and content and recommend that it be accepted in partial fulfillment of the requirements for the degree of Master of Science, with a major in Nuclear Engineering.

Paul N. Stevens, Major Professor

We have read this thesis and
recommend its acceptance:

Accepted for the Council:

Vice Provost
and Dean of the Graduate School

STATEMENT OF PERMISSION TO USE

In presenting this thesis in partial fulfillment of the requirements for a Master's degree at the University of Tennessee, Knoxville, I agree that the Library shall make it available to borrowers under rules of the Library. Brief quotations from this thesis are allowable without special permission, provided that accurate acknowledgment of the source is made.

Permission for extensive quotation from or reproduction of this thesis may be granted by my major professor or, in his absence, by the Head of Interlibrary Services when, in the opinion of either, the proposed use of the material is for scholarly purposes. Any copying or use of the material in this thesis for financial gain shall not be allowed without my written permission.

Signature Wesley E. Bryan

Date 10/29/87

DESIGN OF COMPACT LOOP ANTENNAS FOR PRESENT AND FUTURE FUSION HEATING EXPERIMENTS

A Thesis

Presented for the

Master of Science

Degree

The University of Tennessee, Knoxville

Wesley E. Bryan

December 1987

ACKNOWLEDGMENTS

Development of this thesis was inherently coupled with actual Oak Ridge National Laboratory (ORNL) project goals and timetables. Appreciation is extended to my major professor, Paul Stevens, for his understanding and acceptance of priorities.

My opportunities in this project would not have been possible except for the dedicated work of members of the RF Development Group at ORNL. In particular, I would like to thank Wally Baity, Tom Owens, and Dan Hoffman, who served as my director at ORNL.

Special thanks go to Jim Walters, who generated the mechanical assembly drawings from which many of the figures in this thesis were derived.

ABSTRACT

The goal of the supplemental radio-frequency (rf) heating of fusion plasmas is to deliver power at high efficiencies deep within the plasma interior. Because the different plasma particle species give rise to a range of characteristic resonance frequencies, many options are available for heating a plasma through the absorption of energy from rf waves. Ion cyclotron resonant heating (ICRH) is one of the prime candidates for supplementary heating. The technology of ICRH has reached the point of requiring "proof-of-performance" demonstrations of specific antenna designs. A functional understanding and utilization of aspects of plasma engineering, electrical engineering, and mechanical engineering are necessary to design and evaluate ICRH antennas. The objective of this thesis is to identify these aspects and demonstrate their integration into the design process of a compact loop antenna.

The feasibility of wave excitation and energy deposition to a plasma can be established from the theories of plasma physics. The coupling and propagation, specifically of ICRH waves, are described. Once the theoretical rationale of ICRH is established, a logical progression toward the technology of its implementation is presented.

ICRH antennas can have different electrical configurations, each with characteristic advantages and limitations. A review of past and presently pursued concepts is presented, along with a comparison of the operating parameters for these concepts. Ultimately, the choice of a specific configuration will depend on the technological feasibility of achieving adequate coupling, lifetime, and reliability.

The technology of rf antennas is governed by a closely meshed interaction between electrical and mechanical requirements and constraints. The design of the Oak Ridge National Laboratory (ORNL) version of the antenna configuration

chosen for the Tokamak Fusion Test Reactor (TFTR) is used to characterize rf antenna technology.

As with any design process, the requirements and target parameters are first defined. These design criteria are presented in terms of plasma, electrical, and mechanical considerations. Once the requirements are established, a comprehensive description of the antenna configuration and the functional purpose of individual components is presented. Individual components are evaluated for specific functionality as dictated by electrical, thermal, structural, and material compatibility requirements.

The rf technology developed for present fusion experiments must be extended for the design of antennas of future devices. These future machines will impose new requirements that must be addressed. The final subject is a survey of future antenna design considerations as an extension of present technology, including reactor-relevant plasma heating and nuclear environments.

TABLE OF CONTENTS

LIST OF FIGURES

INTRODUCTION

The fundamental requirement for the production of usable power from the fusion of ionized plasma atoms is to heat a sufficiently dense plasma to ignition temperatures while confining it long enough to produce more energy than was required for ignition. The international fusion research community has successfully developed several magnetic field confinement geometries of which the tokamak is the leading candidate. Currently, pellet injectors are the method of choice for fueling a plasma to sufficient particle densities. Bulk plasma heating requirements have reached a point requiring the technological development of additional supplemental heating devices.

Raising the temperature of a potentially unstable plasma requires that energy inputs occur in a time scale consistent with the particle confinement time while energy dissipation is held to a minimum. Consequently, the heating rate and energy confinement time are the fundamental parameters to be considered in establishing bulk plasma heating requirements. The heating rate is intrinsically associated with technological limitations of the delivery mechanism, and the energy confinement time can be enhanced by energy deposition deep within the plasma.

Resistive heating of the plasma by passing a current through it is an integral part of tokamak operation and provides the primary plasma heating mechanism. However, as the temperature is raised, the resistivity of the plasma decreases, and an increased current is required to effect the same rate of ohmic heating. As the current is raised, plasma magnetohydrodynamic instabilities degrade confinement time, creating an upper bound on the plasma temperature achievable by resistive heating. Consequently, the development of supplemental heating mechanisms becomes a requirement.

Neutral-beam injectors are the most successful means of supplemental heating to date. These devices inject energetic neutral particles through the confining magnetic field, where the particles transfer their energies to the plasma by Coulomb scattering. Neutral beams, however, have several disadvantages. The device has limited efficiency; the energy that does reach the plasma is deposited primarily at the plasma edge, and confinement time is thereby limited. Also, the use of neutral beams does not extrapolate favorably to the power requirements of future fusion reactors.

Another class of supplemental heating mechanisms has been conceived which transfers energy to the plasma through the use of externally generated electromagnetic waves. Theoretically, there are a number of particle resonances that exist in a plasma that is confined in a magnetic field. Some resonances are embodied in the characteristic frequency with which a charged plasma particle orbits a magnetic field line. Some of these resonances occur deep within the plasma where the core heating is required and the net confinement is generally maximum. The particle gyrofrequency, ω, is a function of the local field strength and is defined by

$$\omega = \left| \frac{qB}{m} \right| ,$$

where

q = charge of the particle,

B = local magnetic field strength,

m = mass of the particle.

The frequencies of interest for direct fuel heating encompass those of the plasma ions and are termed ion cyclotron resonance frequencies (ICRFs) or, more generally, ion cyclotron range of frequencies (ICRFs). For magnetic field strengths of several teslas, the ion cyclotron frequencies, Ω_i, fall in the radio-frequency (rf) category.

The generation of rf waves using an antenna at the plasma edge has been experimentally verified in contemporary machines, resulting in limited but significant plasma heating.[1,2] Consequently, ion cyclotron resonant heating (ICRH) has received increasing attention as a prime candidate for supplemental plasma heating. The technology of ICRH has reached the point of requiring "proof-of-performance" demonstrations of specific antenna designs.

To evaluate qualitatively the technological nature of an ICRH antenna, an understanding of the interrelations of plasma engineering, electrical engineering, and mechanical engineering is required. To date, research and development in each discipline have provided the discrete tools prerequisite to the design of an ICRH launcher. The present emphasis of ICRH technology requires the synthesis of concepts with developmental hardware into the design of multimegawatt antenna structures. The Oak Ridge National Laboratory (ORNL) resonant double loop (RDL) antenna has reached the point of being a self-consistent design capable of demonstrating the adequacy of the compact loop concept for present and future supplemental heating requirements. This thesis develops an understanding of the interrelations of the plasma, electrical, and mechanical criteria integrated into the design of the ORNL RDL antenna.

---

[1] M. P. Evrard et al., "Comparison of Theoretical and Experimental ICRF Antenna-Plasma Coupling Resistance in JET," p. 133 in *Proceedings of 13th European Conference on Controlled Fusion and Plasma Heating, Schliersee, April 1986*, Contributed Papers, Part 2, European Physical Society, Schliersee, Germany, 1986.

[2] R. R. Weynants et al., "Power Deposition Profiles in Textor Under ICRH Mode Conversion Conditions," ibid., p. 33.

CHAPTER I

RF PLASMA WAVE PHYSICS

The function of the ICRH antenna is to physically excite an rf wave in the low-particle-density region at the plasma outer edge. The energy associated with the rf wave is stored in the wave electric and magnetic fields. This energy can, in principal, propagate within the plasma wave fields until resonance conditions with a plasma particle are encountered. At resonance, the energy is readily transferred to the particle.

Coupling, Propagation, and Particle Interaction

In the classical sense, the magnetic field associated with a current-carrying circuit element can induce an electric field in other circuits linked by the magnetic field. Two circuits linked by the same magnetic field are coupled to each other. Coupling between two closed circuits permits the transfer of energy between the circuits through the medium of the mutual magnetic field. This phenomenon is the basis on which all transformers operate.

The radiating element of the antenna and the plasma particles are analogous, respectively, to the primary and secondary windings of a transformer circuit. The mutual magnetic field coupling the two is the mechanism by which energy is transferred from the antenna to the plasma.

Conceptually, the very nature of charged particles in motion represents a circuit in which, at least over a restricted space, an electric field can be induced by a magnetic flux. This magnetic flux can mutually couple the particles to another circuit, i.e., the antenna radiating element. The induced electric field would be superimposed on the electric field associated with the natural motion of the particles. Since a charge in motion creates its local magnetic field, the perturbation in the electric field produces a perturbation in the local magnetic field which, in turn, represents a flux that is mutually linking surrounding particles. The process thereby represents a medium for propagation of the induced rf wave through the plasma.

Plasma-to-antenna coupling is a phenomenon not rigorously understood. There is currently an intensive theoretical investigation of this experimentally verifiable phenomenon. A variety of electromagnetic waves possessing individual characteristics can be coupled at the plasma edge. The two ICRF waves of interest are the "fast" and the "slow" waves, differing primarily in their polarization and relative phase velocity. As shown through the cold-plasma model, the slow wave is the primary mechanism by which energy is transferred to the ions. The fast wave, however, is the most practical wave to launch and the most successful at propagating through the plasma.

The fast wave is launched and it propagates around the torus to the center of the plasma, where it encounters a mode conversion surface. At this surface, the fast wave converts into a slow wave. The slow wave then deposits its energy into the "tail" of the energy distribution of a minority ion species, such as hydrogen. Through collisions with the remainder of the distribution, the energy in the tail is transferred to neighboring particles, including those of interest, i.e., deuterium and tritium.

The theory of ICRH heating including the effects of a hot plasma is beyond the scope of this investigation. However, the theory of wave propagation within a cold-plasma model is developed.

Cold-Plasma Dispersion Relation[3]

The cold-plasma model provides a method of mathematical analysis of a plasma which is rooted in the fluid description of a homogeneous system of ions and electrons at zero absolute temperature in a uniform magnetic field. The frequencies of wave phenomena covered by the cold-plasma model lie below the electron cyclotron frequency, and collisions are the only dissipative effects included. Within these physical restrictions, the model is an accurate description of the corresponding waves in a hot plasma.

Fundamental fusion plasma physics examines the interaction of charged particles with electric and magnetic fields. In a stochastic fashion, the motion of a charged particle induces fields which, in turn, initiate forces that influence the particle's motion. Dynamically, the self-consistent interactions of the mechanisms that shape particle motion represent a system in which small-amplitude oscillations, or waves, can be expected to exist and play their own role in shaping the collective motion. If the particle densities and velocities are known, the collective particle motions are ultimately described by the Maxwell equations.

The description of plasma particle motion originates from the requirement that the electric, $\vec{E}(\vec{r},t)$, and magnetic, $\vec{B}(\vec{r},t)$, field vectors satisfy the Maxwell equations. The Maxwell-Faraday law,

$$\oint_{C} \vec{E} \cdot d\vec{\ell} = -\int_{S} \frac{\partial B}{\partial t} \cdot d\vec{S} \ , \tag{1}$$

states that the electromotive force around any closed contour (i.e., the work that would be done by the electric field in moving a unit positive charge once around

[3]N. A. Uckan, class notes on fusion physics, engineering, and technology, The University of Tennessee, Knoxville.

the contour) is equal to the time rate of change of the magnetic flux through an arbitrary surface linking the contour. The Maxwell-Ampere law,

$$\oint_C \vec{H} \cdot d\vec{\ell} = \int_S \left(\vec{J} + \frac{\partial \vec{D}}{\partial t} \right) \cdot d\vec{S} \ , \tag{2}$$

states that the magnetomotive force around any closed contour (i.e., the work that would be done by the magnetic field in moving a unit positive charge once around the contour) is equal to the total flow of current plus the time rate of change of electric flux density out of an arbitrary surface linking the contour.

Stokes' integral theorem converts the line integrals of Eqs. (1) and (2) into surface integral forms. Equation (1) becomes

$$\oint_C \vec{E} \cdot d\vec{\ell} = \int_S (\vec{\nabla} \times \vec{E}) \cdot d\vec{S} = -\int_S \frac{\partial \vec{B}}{\partial t} \cdot d\vec{S} \ ,$$

and, since the surface is arbitrary, the result is the differential form

$$\vec{\nabla} \times \vec{E} = -\frac{\partial \vec{B}}{\partial t} \ . \tag{3}$$

Similarly, Eq. (2) becomes

$$\oint_C \vec{H} \cdot d\vec{\ell} = \int_S (\vec{\nabla} \times \vec{H}) \cdot d\vec{S} = \int_S \left(\vec{J} + \frac{\partial \vec{D}}{\partial t} \right) \cdot d\vec{S} \ ,$$

and the arbitrary nature of the surface results in the differential form

$$\vec{\nabla} \times \vec{H} = \vec{J} + \frac{\partial \vec{D}}{\partial t} \ . \tag{4}$$

The magnetic intensity, $\vec{H}$, is related to the magnetic flux density, $\vec{B}$, through the magnetic permeability of the region, μ, as defined by

$$\vec{B} \equiv \mu \vec{H} \ . \tag{5}$$

The electric flux density, $\vec{D}$, is related to the electric intensity, $\vec{E}$, through the region dielectric permeability, ϵ, as defined by

$$\vec{D} \equiv \epsilon \vec{E} \ . \tag{6}$$

In a vacuum, μ_0 and ϵ_0 are constants and are related by

$$\frac{1}{\mu_0 \epsilon_0} = c^2 \ , \tag{7}$$

where c is the speed of light.

Substituting Eqs. (5) through (7) into Eq. (4) results in

$$\vec{\nabla} \times \vec{B} = \mu_0 \vec{J} + \frac{1}{c^2} \frac{\partial \vec{E}}{\partial t} \ . \tag{8}$$

Equations (3) and (8) represent the differential forms of the Maxwell equations relating the electric and magnetic field vectors. The methodology employed in the cold-plasma model is to derive the wave equation for a cold, magnetized plasma from these differential forms of the Maxwell equations.

The wave equation is simply obtained by taking the curl of Eq. (3) and eliminating $\vec{B}$ with Eq. (8) to yield

$$\vec{\nabla} \times (\vec{\nabla} \times \vec{E}) = -\frac{\partial}{\partial t} \left(\mu_0 \vec{J} + \frac{1}{c^2} \frac{\partial \vec{E}}{\partial t} \right) \ . \tag{9}$$

A relation between $\vec{E}$ and $\vec{J}$ is obtained from the solution of the fluid equations of motion of a plasma. This relation leads to a solution of the wave equation relating the wave propagation vector, $\vec{k}$, to the wave frequency, ω, i.e., $\vec{k}(\omega)$ or $\omega(\vec{k})$.

Since the magnitude of an accurate stochastic description of a plasma behavior based on the trajectories of individual particles is prohibitive, solution of plasma kinetics is based on deterministic methods. Taking the total derivative of the distribution function, $f(\vec{v}, \vec{r}, t)$, with respect to time results in the plasma kinetic equation. The expected values represented by this differential equation when solved as multiple powers of the velocity vector result in the distribution function moments (moments equations). The equation for the first moment represents the conservation of momentum.

The multifluid conservation-of-momentum equation with heat conduction and collisions omitted and assuming a scalar base pressure, P, takes on the form

$$m_j n_j \frac{dv_j}{dt} = -\vec{\nabla} P_j + n_j q_j (\vec{E} + \vec{v}_j \times \vec{B}) \ . \tag{10}$$

A linearized equation of motion can be developed, with equilibrium quantities denoted by subscript 0 and perturbed quantities by subscript 1. Further assumptions of a uniform neutral plasma at rest and the cold-plasma model restriction of zero temperature result in the following moment equation:

$$m_j \frac{\partial v_{1j}}{\partial t} = q_j (\vec{E}_1 + \vec{v}_{1j} \times \vec{B}_0) \ . \tag{11}$$

Derivation of a relation between $\vec{E}$ and $\vec{J}$ is a multistep procedure beginning with Eq. (11). Let the perturbed quantities in Eq. (11) take a sinusoidally oscillating form, e.g.,

$$\vec{v}_1 = \vec{v}_0 \exp[\mathrm{i}(\vec{k} \cdot \vec{r} - \omega t)] \ ; \tag{12}$$

then

$$\frac{\partial v_{1j}}{\partial t} = -\mathrm{i}\omega \vec{v}_{1j} \ . \tag{13}$$

If B_0 is aligned along the z-axis, with x and y components vanishing, and with

$$\Omega_j = \left| \frac{q_j B_0}{m_j} \right| > 0 \ ,$$

$$\sigma_j = +1 \text{ for ions } (q_j > 0) \ ,$$

and

$$\sigma_j = -1 \text{ for electrons } (q_j < 0) \ ,$$

Eq. (11) can be split into orthogonal components. The resulting component equations can be simultaneously solved to yield the following components of $\vec{v}_j$ as linear functions of $\vec{E}$:

$$v_{jx} = \frac{\mathrm{iE_x}}{\mathrm{B_0}} \frac{\sigma_j \Omega_j \omega}{\omega^2 - \Omega_j^2} - \frac{E_y}{B_0} \frac{\Omega_j^2}{\omega^2 - \Omega_j^2} , \tag{14a}$$

$$v_{jy} = \frac{E_x}{B_0} \frac{\Omega_j^2}{\omega^2 - \Omega_j^2} + \frac{\mathrm{iE_y}}{\mathrm{B_0}} \frac{\sigma_j \Omega_j \omega}{\omega^2 - \Omega_j^2} , \tag{14b}$$

and

$$v_{jz} = \frac{\mathrm{i}E_z}{\omega} . \tag{14c}$$

At this point, a relation between $\vec{v}_j$ and $\vec{J}$ is derived from the definition of the current density,

$$\vec{J} \equiv \sum_j \rho_j v_j = \sum_j q_j n_j \vec{v}_j . \tag{15}$$

Substituting Eq. (14) into Eq. (15) and incorporating the definition of plasma oscillations,

$$\omega_{\mathrm{p}j}^2 \equiv \frac{1}{\epsilon_0} \sum_j \frac{n_j q_j^2}{m_j} , \tag{16}$$

results in the following equations for the components of $\vec{J}$:

$$J_x = \left(\epsilon_0 \sum_j \frac{\omega_{\mathrm{p}j}^2 \mathrm{i}\omega}{\omega^2 - \Omega_j^2} \right) E_x - \left(\epsilon_0 \sum_j \frac{\omega_{\mathrm{p}j}^2 \sigma_j \Omega_j}{\omega^2 - \Omega_j^2} \right) E_y + 0 , \tag{17a}$$

$$J_y = \left(\epsilon_0 \sum_j \frac{\omega_{\mathrm{p}j}^2 \sigma_j \Omega_j}{\omega^2 - \Omega_j^2} \right) E_x + \left(\epsilon_0 \sum_j \frac{\omega_{\mathrm{p}j}^2 \mathrm{i}\omega}{\omega^2 - \Omega_j^2} \right) E_y + 0 , \tag{17b}$$

$$J_z = 0 + 0 + \left(\epsilon_0 \sum_J \frac{\omega_{\mathrm{p}j}^2 \mathrm{i}\omega}{\omega} \right) E_z . \tag{17c}$$

With the conductivity tensor, $\overleftrightarrow{\sigma}$, Eq. (17) can be written in matrix form as

$$\begin{pmatrix} J_x \\ J_y \\ J_z \end{pmatrix} = \begin{pmatrix} \sigma_{xx} & \sigma_{xy} & \sigma_{xz} \\ \sigma_{yx} & \sigma_{yy} & \sigma_{yz} \\ \sigma_{zx} & \sigma_{zy} & \sigma_{zz} \end{pmatrix} \begin{pmatrix} E_x \\ E_y \\ E_z \end{pmatrix}$$

or simply as

$$\vec{J} = \overleftrightarrow{\sigma} \cdot \vec{E} . \tag{18}$$

Equation (18) provides a relation between $\vec{J}$ and $\vec{E}$. Now, inserting Eq. (18) back into Eq. (9) yields the wave equation in terms of the conductivity tensor:

$$\vec{\nabla} \times (\vec{\nabla} \times \vec{E}) = -\left[\frac{\partial}{\partial t}(\mu_0 \overleftrightarrow{\sigma} \cdot \vec{E}) + \frac{1}{c^2}\frac{\partial}{\partial t}\frac{\partial \vec{E}}{\partial t}\right] . \tag{19}$$

Expanding each term of Eq. (19), while remembering that perturbed quantities have the form of Eq. (12), and using the following identity in the first term,

$$\vec{A} \times \vec{B} = (A_y B_z - A_z B_y)\hat{i} + (A_z B_x - A_x B_z)\hat{j} + (A_x B_y - A_y B_x)\hat{k} ,$$

yields the following form of the wave equation:

$$\mathrm{i}\vec{k} \times (\mathrm{i}\vec{k} \times \vec{E}) = -\left(-\mathrm{i}\omega\mu_0 \overleftrightarrow{\sigma} \cdot \vec{E} - \frac{1}{c^2}\omega^2 \vec{E}\right) . \tag{20}$$

With $\mu_0 = (1/\epsilon_0 c^2)$ and identity $i^2 = -1$ substituted into Eq. (20), the wave equation becomes

$$-\vec{k} \times (\vec{k} \times \vec{E}) = \frac{\omega^2}{c^2}\vec{E} + \frac{\omega^2}{c^2}\left(\frac{\mathrm{i}\overleftrightarrow{\sigma}}{\epsilon_0 \omega}\right)\vec{E} . \tag{21}$$

Factoring Eq. (21) further and introducing the unit tensor, $\overleftrightarrow{I}$, results in

$$-\vec{k} \times (\vec{k} \times \vec{E}) = \frac{\omega^2}{c^2}\left(\overleftrightarrow{I} + \frac{\mathrm{i}\overleftrightarrow{\sigma}}{\omega\epsilon_0}\right) \cdot \vec{E} , \tag{22}$$

where the dielectric tensor is defined as

$$\overleftrightarrow{\epsilon} \equiv \overleftrightarrow{I} + \frac{I\overleftrightarrow{\sigma}}{\omega\epsilon_0} . \tag{23}$$

The wave equation, expressed in terms of the dielectric tensor, becomes

$$\vec{k} \times (\vec{k} \times \vec{E}) + \frac{\omega^2}{c^2}\overleftrightarrow{\epsilon} \cdot \vec{E} = 0 . \tag{24}$$

The components of $\overleftrightarrow{\epsilon}$ can be obtained by inserting the components of $\overleftrightarrow{\sigma}$, as defined in Eq. (17), into Eq. (23). With

$$\epsilon_1 \equiv \epsilon_{xx} = 1 - \sum_j \frac{\omega_{pj}}{\omega^2 - \Omega_j^2} \ , \tag{25a}$$

$$-\mathrm{i}\epsilon_2 \equiv \epsilon_{xy} = -\mathrm{i} \left[\sum_j \left(\frac{\sigma_j \Omega_j}{\omega} \right) \frac{\omega_{pj}^2}{\omega^2 - \Omega_j^2} \right] \ , \tag{25b}$$

and

$$\epsilon_3 \equiv \epsilon_{zz} = 1 - \sum_j \frac{\omega_{pj}^2}{\omega^2} \ , \tag{25c}$$

the components of $\overleftrightarrow{\epsilon}$, written in matrix form, become

$$\begin{pmatrix} \epsilon_1 & -\mathrm{i}\epsilon_2 & 0 \\ \mathrm{i}\epsilon_2 & \epsilon_1 & 0 \\ 0 & 0 & \epsilon_3 \end{pmatrix} . \tag{26}$$

If each term of Eq. (24) is expanded with Eqs. (25) and (26), while $\vec{k}$ is defined as lying in the x–z plane so that $k_y = 0$, $k_x = k \sin\theta$, and $k_z = k \cos\theta$, where θ is the angle between $\vec{B}_0 = B_0 \hat{e}_z$ and $\vec{k}$, the wave equation in component form is given by

$$\begin{aligned} \hat{i} &: \left[-k^2 \cos\theta + \frac{\omega^2}{c^2}\epsilon_1 \right] E_x - \left[\frac{\omega^2}{c^2}\mathrm{i}\epsilon_2 \right] E_y + [k^2 \cos\theta \sin\theta] E_z = 0 \ , \\ \hat{j} &: \left[\frac{\omega^2}{c^2}\mathrm{i}\epsilon_2 \right] E_x + \left[-k^2 + \frac{\omega^2}{c^2}\epsilon_1 \right] E_y + 0 E_z = 0 \ , \\ \hat{k} &: [k^2 \cos\theta \sin\theta] E_x + 0 E_y + \left[-k^2 \sin^2\theta + \frac{\omega^2}{c^2}\epsilon_3 \right] E_z = 0 \ . \end{aligned} \tag{27}$$

If each term of Eq. (27) is multiplied by (c^2/ω^2) and the refractive index, $\eta^2 \equiv (k^2 c^2/\omega^2)$, is introduced, the wave equation in matrix form becomes

$$\begin{pmatrix} \epsilon_1 - \eta^2 \cos^2\theta & -\mathrm{i}\epsilon_2 & \eta^2 \sin\theta\cos\theta \\ \mathrm{i}\epsilon_2 & \epsilon_1 - \eta^2 & 0 \\ \eta^2 \sin\theta\cos\theta & 0 & \epsilon_3 - \eta^2 \sin^2\theta \end{pmatrix} \begin{pmatrix} E_x \\ E_y \\ E_z \end{pmatrix} = 0 \ . \tag{28}$$

The derivation of Eq. (28) has been general within the context of the cold-plasma model. The general solution of Eq. (28) provides a general dispersion relation between ω and $\vec{k}$. This relation can be examined in specific frequency ranges to yield information about the various wave types and their physical attributes and interactions within the plasma system. However, at this point, an approximate solution to the wave equation will be developed for frequencies around the ion cyclotron ($\Omega_{\rm i}$) range of frequencies.

Equation (28) can be rewritten as

$$\begin{pmatrix} \epsilon_1 - \eta_\parallel^2 & -{\rm i}\epsilon_2 & \eta_\parallel \eta_\perp \\ {\rm i}\epsilon_2 & \epsilon_1 - \eta^2 & 0 \\ \eta_\perp \eta_\parallel & 0 & \epsilon_3 - \eta_\perp^2 \end{pmatrix} \begin{pmatrix} E_x \\ E_y \\ E_z \end{pmatrix} = 0 \ , \tag{29}$$

where $\eta_\perp = \eta \sin\theta$ and $\eta_\parallel = \eta\cos\theta$.

In the ion cyclotron range of frequencies $\omega^2 \sim \Omega_{\rm i}^2 \ll \Omega_{\rm e}^2$, $\omega_{\rm pe}^2$ and for a one-species plasma, the components of the dielectric tensor can be approximated from Eq. (25) as

$$\epsilon_1 \approx 1 - \frac{\omega_{\rm pi}^2}{\Omega_{\rm i}^2} \frac{\Omega_{\rm i}^2}{\omega^2 - \Omega_{\rm i}^2} \approx \frac{\omega_{\rm pi}^2}{\Omega_{\rm i}^2} \frac{\Omega_{\rm i}^2}{\Omega_{\rm i}^2 - \omega^2} \ , \tag{30a}$$

$$\epsilon_2 \approx \frac{\omega_{\rm pi}^2 \omega}{\Omega_{\rm i}(\omega^2 - \Omega_{\rm i}^2)} \approx \frac{\omega_{\rm pi}^2}{\Omega_{\rm i}^2} \frac{\omega \Omega_{\rm i}}{\omega^2 - \Omega_{\rm i}^2} \ , \tag{30b}$$

$$\epsilon_3 \approx 1 - \frac{\omega_{\rm pe}^2}{\omega^2} \approx -\frac{\omega_{\rm pe}^2}{\omega^2} \ . \tag{30c}$$

Since $\omega^2 \ll \omega_{\rm pe}^2$, it is apparent from Eq. (30c) that ϵ_3 is the largest element in the dielectric tensor. Then, for the E_z component,

$$\eta_\perp \eta_\parallel E_x + (\epsilon_3 - \eta_\perp^2) E_z = 0 \ . \tag{31}$$

Since the term containing ϵ_3 is dominant, Eq. (31) can be approximated by

$$(\epsilon_3 - \eta_\perp^2) E_z = 0 \ , \tag{32}$$

which leads to the conclusion that $E_z \approx 0$.

The preceding interpretation is known as the low-frequency, high-conductivity approximation, assuming that the high conductivity of the plasma shorts out the parallel electric field. With $E_z \approx 0$ and with terms rearranged, Eq. (29) in component form becomes

$$(\epsilon_1 - \eta_\parallel^2)E_x + (i\epsilon_2)E_y = 0 \ , \tag{33a}$$

$$(-i\epsilon_2)E_x + (\epsilon_1 - \eta^2)E_y = 0 \ . \tag{33b}$$

Multiplying Eq. (33a) by $(\epsilon_1 - \eta^2)$ and Eq. (33b) by $(i\epsilon_2)$ allows a simultaneous solution that results in

$$(\epsilon_1 - \eta_\parallel^2)(\epsilon_1 - \eta^2) - (-i\epsilon_2)(i\epsilon_2) = 0 \ . \tag{34}$$

Since $\eta^2 = (k^2c^2/\omega^2)$, if Eq. (34) is multiplied by ω^2/c^2 and the Alfvén velocity $v_A^2 \equiv (c^2\Omega_i^2/\omega_{pi}^2)$ is introduced, the approximated ICRF dispersion relation becomes

$$k_\perp^2(A - k_\parallel^2) - (B - k_\parallel^2)(C - k_\parallel^2) = 0 \ , \tag{35}$$

where

$$A = \frac{\omega^2}{v_A^2}\frac{\Omega_i^2}{\Omega_i^2 - \omega^2} = \left(\frac{\omega^2}{c^2}\right) \epsilon_1 \ ,$$

$$B = \frac{\omega^2}{v_A^2}\frac{\Omega_i}{\Omega_i - \omega} = \left(\frac{\omega^2}{c^2}\right)(\epsilon_1 - \epsilon_2) \ ,$$

$$C = \frac{\omega^2}{v_A^2}\frac{\Omega_i}{\Omega_i + \omega} = \left(\frac{\omega^2}{c^2}\right)(\epsilon_1 + \epsilon_2) \ .$$

Qualitatively significant information can be obtained from the ICRF dispersion relation, Eq. (35), by examining specific cases.

Considering the surface where

$$A - k_\parallel^2 = 0 \tag{36a}$$

leads to the conclusion that

$$k_\perp^2 = \frac{(B - k_\parallel^2)(C - k_\parallel^2)}{0} \to \infty \ . \tag{36b}$$

This defines the ion cyclotron resonance for the perpendicular component of a wave propagation vector since, from the definition

$$\eta_\perp^2 \equiv \frac{k_\perp^2 c^2}{\omega^2} = \frac{c^2}{v_p^2} \ , \tag{37}$$

the refractive index (which is the ratio of the velocity of light to the wave phase velocity) goes to infinity and the perpendicularly propagating portion of the wave can be absorbed by the ions. This condition also leads to two additional observations. The dispersion relation can be reduced to the cases where

$$B - k_\parallel^2 = 0 \ , \tag{38a}$$

leading to the conclusion that

$$k_\parallel^2 = \frac{\omega^2}{v_A^2} \frac{\Omega_i}{\Omega_i - \omega} \ , \tag{38b}$$

and

$$C - k_\parallel^2 = 0 \ , \tag{39a}$$

leading to the conclusion that

$$k_\parallel^2 = \frac{\omega^2}{v_A^2} \frac{\Omega_i}{\Omega_i + \omega} \ . \tag{39b}$$

Equations (38) and (39) suggest the possible coexistence of two different waves. The waves are distinguished by their relative phase velocities as defined by $v_p \equiv \omega/k$.

Inspection of Eqs. (38) and (39) shows that, for all parameters being fixed, Eq. (39) will have a phase velocity greater than Eq. (38). Equation (38) describes the conditions for the slow electromagnetic ion cyclotron wave, and Eq. (39) describes the conditions for the fast magnetosonic wave. In fact, the condition of Eq. (36) also represents a conversion surface where a wave can change between the modes implied by Eqs. (38) and (39).

The conditions of Eqs. (38) and (39) leave the dispersion relation, Eq. (35), in the form

$$k_\perp^2(A - k_\parallel^2) = 0 \ ,$$

leading to the conclusion that

$$k_\perp^2 = 0 \ . \tag{40}$$

Equation (40) indicates that the perpendicularly propagating portion of the slow or fast wave is said to be in a "cutoff" condition since the refractive index becomes zero and the wave is actually reflected. Equation (38) is the cutoff condition for the slow wave, and Eq. (39) is the cutoff condition for the fast wave.

Obviously, the absorption of a wave by ions is concerned with the various resonance conditions. Cyclotron acceleration of ions depends principally on the amplitude of the left-hand circularly polarized component of the wave electric field in the plasma since the rotation of ions around the magnetic field lines is naturally left handed. For general propagation directions, both the slow and the fast waves are elliptically polarized, having a left-hand component $(E_x + \mathrm{i}E_y)$ and a right-hand component $(E_x - \mathrm{i}E_y)$. If Eq. (33) is referenced, the ratio, or degree of ellipticity, can be determined:

$$\begin{aligned} \frac{E_\mathrm{L}}{E_\mathrm{R}} &= \frac{E_x + \mathrm{i}E_y}{E_x - \mathrm{i}E_y} \\ &= \frac{(\epsilon_1 - \eta_\parallel^2) - \epsilon_2}{(\epsilon_1 - \eta_\parallel^2) + \epsilon_2} \\ &= -\frac{(\epsilon_1 + \epsilon_2) - \eta_\parallel^2}{(\epsilon_1 - \epsilon_2) - \eta_\parallel^2} \ . \end{aligned} \tag{41}$$

Defining $\mathrm{R} \equiv \epsilon_1 + \epsilon_2$ to be right circular polarization and $\mathrm{L} \equiv \epsilon_1 - \epsilon_2$ to be left circular polarization results in

$$\frac{E_{\mathrm{L}}}{E_{\mathrm{R}}} = \frac{\eta_{\|}^2 - \mathrm{R}}{\eta_{\|}^2 - \mathrm{L}} . \tag{42}$$

If Eq. (38) is considered for the specific case where $k_\perp = 0$,

$$k_{\|}^2 = B = \frac{\omega^2}{c^2}(\epsilon_1 - \epsilon_2) = \frac{\omega^2}{c^2}(\mathrm{L}) , \tag{43}$$

which shows that the slow wave traveling parallel to the magnetic field is purely left-circularly polarized.

Similarly, Eq. (39) for $k_\perp = 0$ results in

$$k_{\|}^2 = C = \frac{\omega^2}{c^2}(\epsilon_1 + \epsilon_2) = \frac{\omega^2}{c^2}(\mathrm{R}) , \tag{44}$$

which shows that the fast wave traveling parallel to the magnetic field is purely right-circularly polarized.

Inspection of the denominator of Eq. (38) indicates that the slow wave can propagate only below the ion cyclotron frequency ($\omega < \Omega_{\mathrm{i}}$). Inspection of the denominator of Eq. (39) indicates that the fast wave is not dependent on Ω_{i} and can propagate over a wide range of frequencies, but it is primarily right-circularly polarized, as suggested by Eq. (44). Since heating of the ions depends on the left-circularly polarized component of the rf field, the cold-plasma model predicts strong absorption for the slow wave and no heating with the fast wave. In reality, the cold-plasma model is not strictly applicable to the fast wave since the natural spread of ion velocities along the magnetic field broadens the cyclotron resonance and prevents the fast wave polarization from becoming strictly right-hand circular. The residual left-hand circular component heats the ions at cyclotron resonance. Hot-plasma effects and multiple-ion plasmas, not included in the cold-plasma model, also enhance absorption characteristics. Furthermore, the fast wave propagates toward the perpendicular resonance surface of Eq. (36) and mode-converts into the slow wave for greater absorption characteristics.

Limited access between adjacent toroidal field (TF) coils imposes the largest physical restriction in launching waves to the plasma of a tokamak. Launching perpendicularly from the outside edge (low magnetic field side) of the plasma is the most operationally practical. The limited frequency range over which the slow wave can propagate proves to be a serious disadvantage. When launched from the outside edge, a slow wave will experience cutoff before penetrating the plasma to a productive extent. The fast wave, on the other hand, propagates freely over a wide range of frequencies, plasma densities, and wavelengths.

Both waves can be excited at the plasma periphery by magnetic field perturbations, but, in practice, operational utility becomes the most important factor in choosing fast wave launching over the slow wave.

Excitation

The fast wave can be excited by perturbing the particle toroidal magnetic field with a toroidally oriented magnetic field produced by the antenna. The right-hand rule implies that the externally applied field would be produced by a current flowing poloidally. The general relationship is illustrated in Fig. 1.

For the fast wave, as implied in Eq. (32), the plasma rf electric field in the toroidal direction is small, so wave coupling is dominated by magnetic flux linkage along the magnetic field of the tokamak. In order to perturb only this toroidal magnetic field, a Faraday shield is placed between the current strap and the plasma. The shield is a set of toroidally oriented conducting strips to effectively short out any radiating toroidal electric field. This prevents the unwanted polarization from reaching the plasma boundary. The Faraday shield also shields the current strap

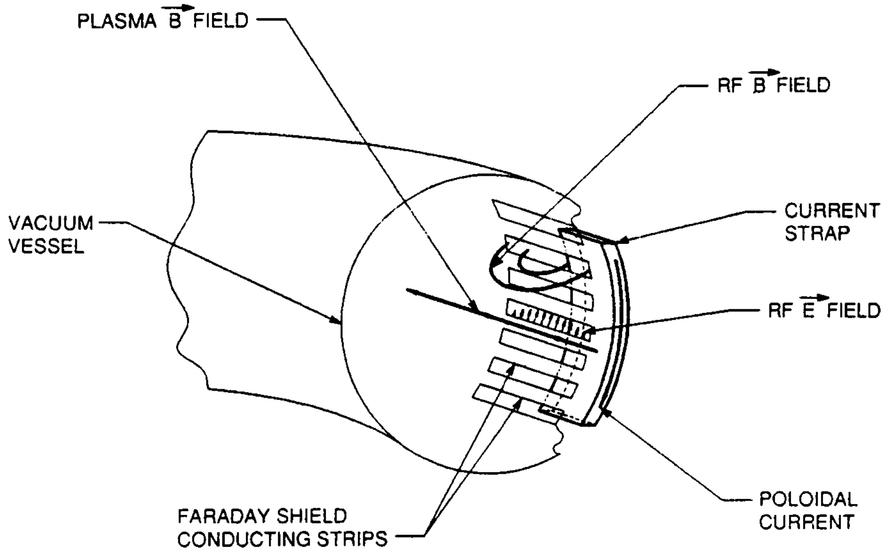

Fig. 1. Fast wave antenna orientation and field pattern.

from the harsh plasma environment while still allowing for efficient flux linkage. A third function of the shield is to "protect" the plasma from sputtering of the high-Z materials, e.g., copper, required in the antenna structure.

CHAPTER II

ELECTRICAL CONFIGURATIONS

The electrical objective of rf technology is to create an external circuit that not only efficiently excites the rf wave at the plasma perimeter but also delivers substantially more power per antenna than present-day experiments. Proof of the applicability of ICRF heating has been accomplished on present experiments with a combined total available power of 1 to 5 MW.

General Requirements

Near-term fusion experiments will require 10 to 50 MW of total power for significant plasma heating. To date, only 0.1 to 0.8 MW per antenna has been achieved. For delivery of more power, the number of ports available to dedicate to antennas and port physical-size limitations dictate maximizing the power delivered per antenna. As part of the National Ion Cyclotron Heating Program, members of the Plasma Technology Group in the ORNL Fusion Energy Division investigated the rf coupling characteristics and capabilities of several antenna configurations.[4] Specific configurations evaluated include the simple loop antenna, the cavity antenna, and the double loop antennas. Results of the investigation include a comparison of the frequency, performance, and power limitations of these representative configurations.

The power deliverable by any antenna is bounded by the simple equations

$$P = I^2 R \; , \tag{45}$$

[4]D. J. Hoffman et al., "Experimental Measurements of the Ion Cyclotron Antennas' Coupling and RF Characteristics," *Fusion Technol.* (Proceedings of the 6th Topical Meeting on the Technology of Fusion Energy, San Francisco, Calif., March 1985) 8(1), 411 (1985).

where

$$R \equiv \text{plasma load} \ ,$$

and

$$P = IV \ . \tag{46}$$

The plasma load, R, is directly proportional to the antenna coupling characteristics—the mechanisms of which are not thoroughly understood. Consequently, R must be treated as an input variable that is best left to experimental determination. For a power supply of limited current capacity, it is evident from Eq. (45) that the deliverable power will be dictated by, and possibly limited by, the plasma load. Furthermore, Eq. (46) shows that, in addition to current, voltage may be physically limited by the antenna components themselves.

Realistically, it is desirable to deliver the most power at the lowest load. If loading is adequate, this will allow the antenna to be withdrawn from the harsh plasma environment, increasing its life and reliability.

Simple Loop Antenna

The simple loop has been one of the most widely used configurations to heat plasmas. A physical schematic of the simple loop shown in Fig. 2 includes a characteristic impedance input rf coaxial line with an rf vacuum feedthrough and an end-fed, half-turn loop current strap shorted at the far end. The corresponding elements in the circuit representation, shown in Fig. 3, are an input impedance, an inductor representing the coupled mutual inductance between the current strap and the plasma, and a plasma loading impedance (resistance) referred to the primary circuit. The circuit parameters of this antenna configuration are as follows:

$$V_{\max} = [R^2 + (\omega L)^2]^{1/2} \ \left(\frac{P}{R}\right)^{1/2} \ , \tag{47}$$

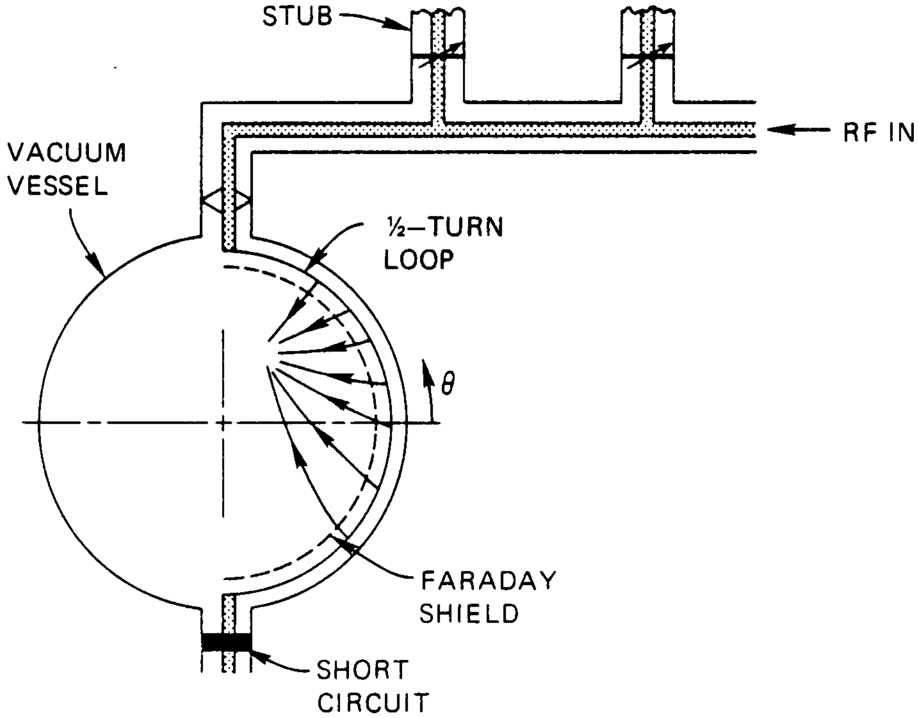

Fig. 2. Simple loop antenna schematic.

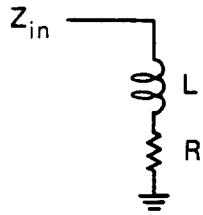

Fig. 3. Simple loop antenna circuit representation.

$$I_{\max} = \left(\frac{P}{R}\right)^{1/2} . \tag{48}$$

The experimental attractiveness of the simple loop configuration lies essentially in the simplicity of its implementation. A simple current strap, surrounded on three sides by a Faraday shield, maximizes the magnetic field away from the antenna, and this leads to good coupling. However, as power per antenna increases, the simple loop encounters technical limitations. The maximum voltage in the circuit occurs at the vacuum feedthrough. Hence, power transmission is limited to the voltage-handling capabilities of the feedthrough. In addition, the maximum current must also pass through the feedthrough, taxing the physical ability of delivering adequate cooling capacity.

Though attractive from an experimental standpoint, the simple loop configuration does not extrapolate favorably to reactor applications. The length of the loop dictates the use of multiple machine ports. Installation is time-consuming and requires much "hands-on-machine" time, which will not be possible once a reactor vessel becomes activated. The use of multiple ports immediately precludes any remote positional adjustment. The length of the loop is also a disadvantage when disruption forces in a reactor-scale device are imposed on the structure.

Cavity Antenna

In an attempt to reduce the physical size of antennas and to facilitate installation, the future antennas are based on the compact loop concept that allows installation through a single port.

The baseline cavity configuration is represented schematically in Fig. 4. The antenna input consists of the characteristic impedance input coaxial line with an rf vacuum feedthrough. Beyond the feedthrough, a lead line penetrates a

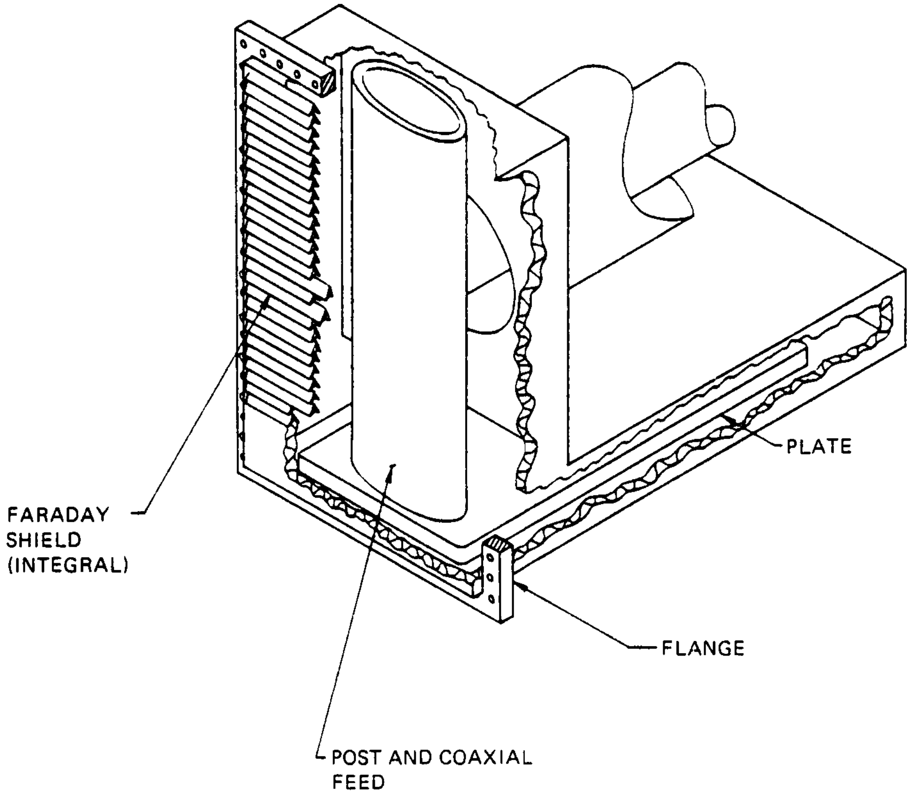

Fig. 4. Cavity antenna schematic.

cavity housing a midsection-fed current strap grounded at one end and integral with a tuning capacitor at the other end. The corresponding circuit elements, shown in Fig. 5, include the input impedance, lead inductance, divided coupling inductance and plasma loading impedance, and a variable capacitance. As with the loop antenna, the maximum circuit current and maximum voltage are given by Eqs. (47) and (48). The remaining circuit parameters are as follows:

$$V_{\text{feedpoint}} = \alpha\omega L \left(\frac{P}{R}\right)^{1/2} , \tag{49}$$

$$C_1 = \frac{1}{\omega^2 L} . \tag{50}$$

On circuit voltage limits ($V_{\max}$), the cavity configuration has the same power capacity as the simple loop. However, the cavity configuration provides the first

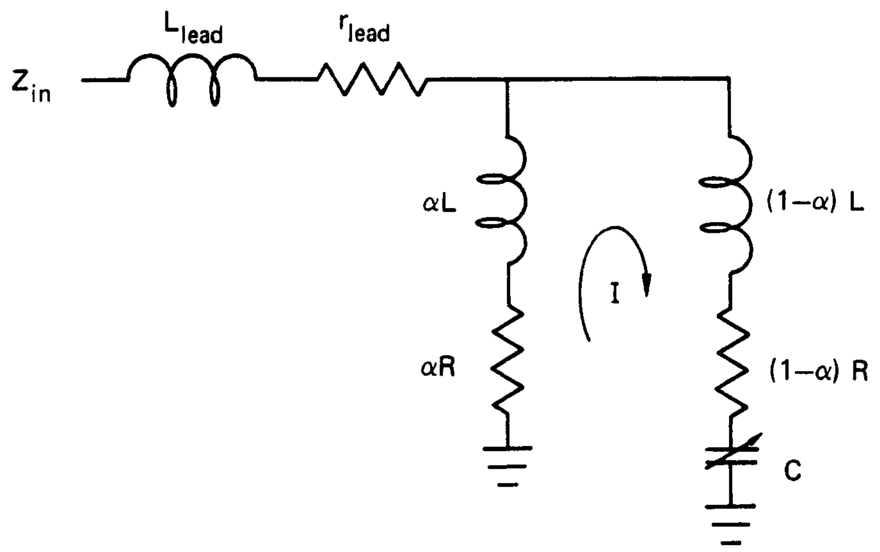

Fig. 5. Cavity antenna circuit representation.

significant improvement over the simple loop. The area of maximum voltage is no longer at the vacuum feedthrough. It now occurs near the ends of the current strap in a shieldable area behind the Faraday shield. This area can sustain the voltages more readily and would lessen the impact to machine operation if a catastrophic voltage breakdown should occur. Consequently, the cavity antenna can have a higher voltage rating than the simple loop.

The proximity of the cavity walls to the current strap has the disadvantage of reducing magnetic fields away from the antenna, but they also can be used to define the induced-wave-mode spectrum ($k_{\|}$ vs $k_{\perp}$). At this time, the optimum mode spectrum is not known, so the emphasis of investigation is driven by technological considerations.

Experimental studies have identified that the cavity antenna is suitable for coupling over a 1- to 5-Ω plasma load range through a 40- to 80-MHz frequency range. Below 1 Ω, 1 MW was not achievable over frequencies of practical interest. Above 5 Ω, the current distributions in the inductive and capacitive legs of the current strap are substantially different. This asymmetry in current distribution precludes the impedance matching capability of the two legs which is desirable for optimal power transmission.

The position of the feedpoint along the current strap is actually integral to the impedance matching at various loads. Since the feedpoint is fixed at fabrication, matching is optimal only at one load. As plasma load changes, the two legs of the strap will be only partially matched. Although the cavity cannot match at all loads, the rf transmission system voltages are still favorably reduced because of the partial matching.

Resonant Double Loop Antennas

The resonant double loop (RDL) configurations are represented schematically in Fig. 6. The antenna contains the same physical components as the cavity configuration with the addition of a second capacitor replacing the grounded end of the current strap. The corresponding circuit elements are shown in Fig. 7. The feature distinguishing the asymmetric RDL from the symmetric RDL is the nonsymmetric feedpoint on the current strap.

As with the simple loop and cavity antennas, the maximum current is given by Eq. (47). The remaining circuit parameters for the symmetric RDL are as follows:

$$V_{\max} \approx \sqrt{\frac{P}{R}} \left(\alpha \omega L + \sqrt{R Z_0} \right) \ , \tag{51}$$

where $\alpha \geq 0.5$,

$$V_{\text{feedpoint}} \approx \sqrt{P Z_0} \ , \tag{52}$$

$$C_1 \approx \left[\omega \left(\alpha \omega L - \sqrt{R Z_0} \right) \right]^{-1} \ , \tag{53}$$

$$C_2 \approx \left\{ \omega \left[(1-\alpha) \omega L + \sqrt{R Z_0} \right] \right\}^{-1} \ . \tag{54}$$

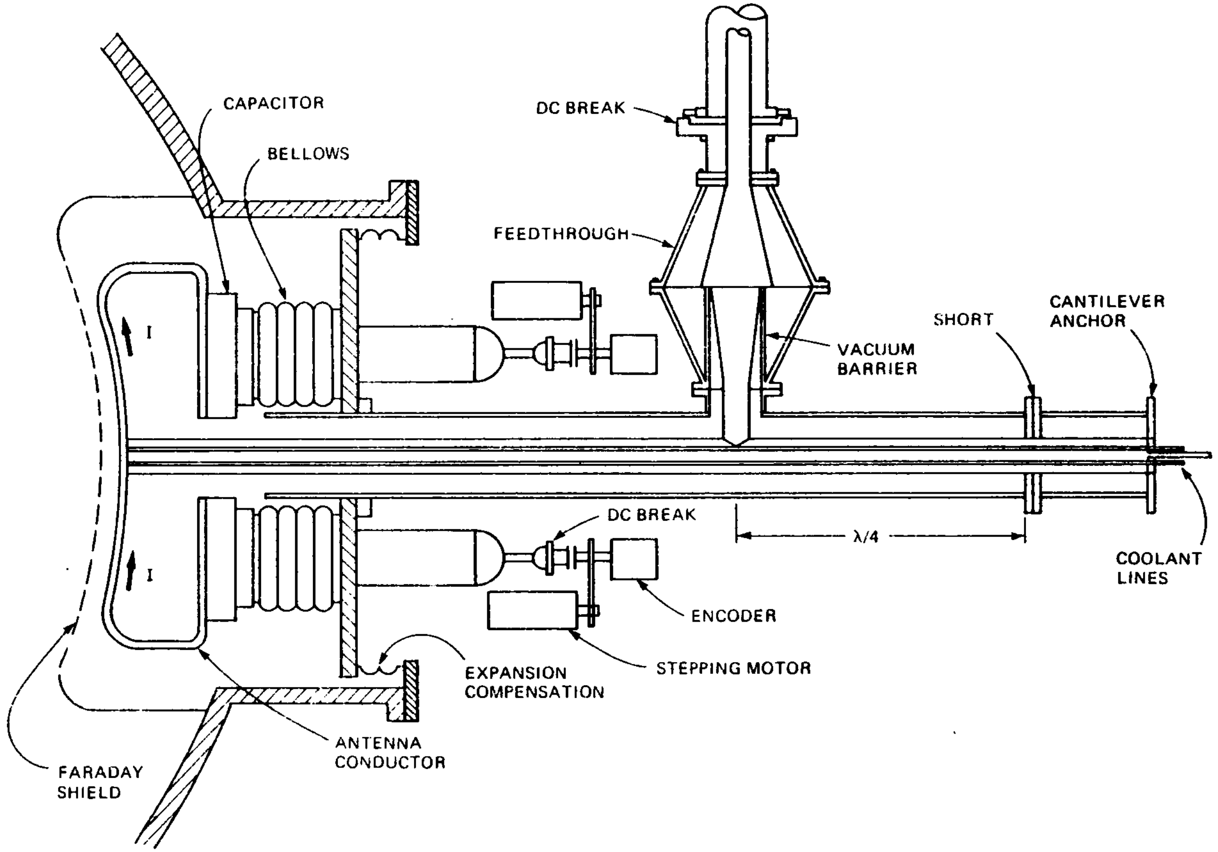

Fig. 6. RDL antenna schematic.

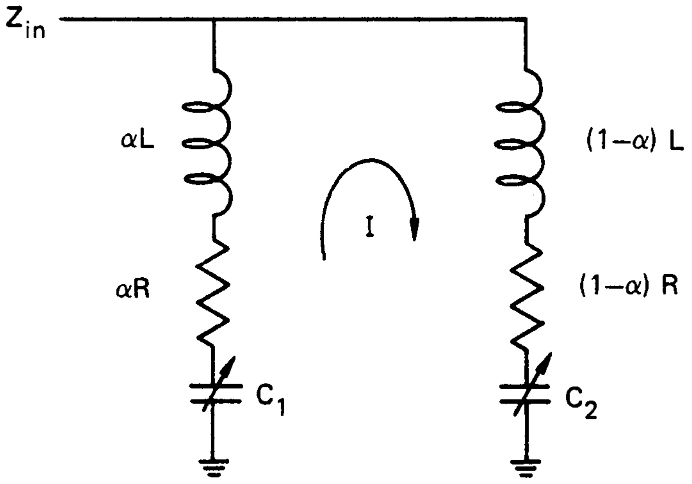

Fig. 7. RDL antenna circuit representation.

The corresponding circuit parameters for the asymmetric RDL must be determined computationally.[5] A distributed, "lossy," coaxial-transmission-line model (shown in Fig. 8) is used for the calculations. The voltages and currents on various elements have been computed as functions of plasma load for a given antenna power and plotted in Fig. 9.

In addition to the high-voltage relocation benefits of the cavity antenna, the RDL can operate at the same power per antenna in a lower load range. In fact, at low loads, the RDL cuts voltages to ground in half and therefore allows four times the power capability of the cavity. Furthermore, the RDL can be matched at different loads and frequencies, with matching limitations only at certain upper loads.

The asymmetric RDL antenna offers the most flexibility in delivering maximum power per antenna while accommodating the uncertainties associated with

[5] D. J. Hoffman et al., "The Design of High-Power ICRF Antennas for TFTR and Tore Supra," to be published in the Proceedings of the 7th Topical Conference on Applications of Radio-Frequency Power to Plasmas, Kissimmee, Fla., May 1987.

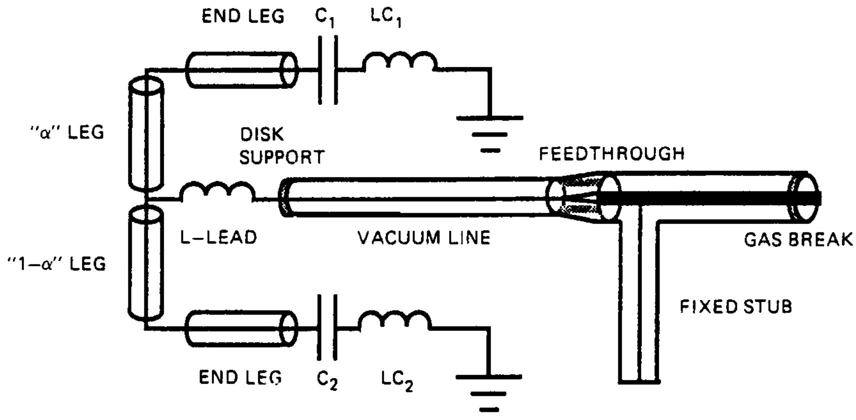

Fig. 8. ORNL RDL antenna circuit model.

antenna to plasma coupling, antenna erosion, and reliability. This flexibility allows the operator to retract the antenna and work at lower but still significant power or to insert fully and operate at power densities that would test the mechanical limits of the antenna structure itself.

A program to implement ICRH in the Tokamak Fusion Test Reactor (TFTR) at Princeton Plasma Physics Laboratory (PPPL) was recently initiated. Fortunately, the machine offers ORNL the opportunity to design an asymmetric RDL antenna and demonstrate the supplemental heating performance capabilities of this compact loop antenna concept.

	Current strap	End lines	Disk support
Z_0, Ω	66.0	73.0	17.1
R/L, Ω/m	6.000	0.010	0.000
v_{phase}/c	0.650	0.950	0.343
Length, m	0.640	0.300	0.025

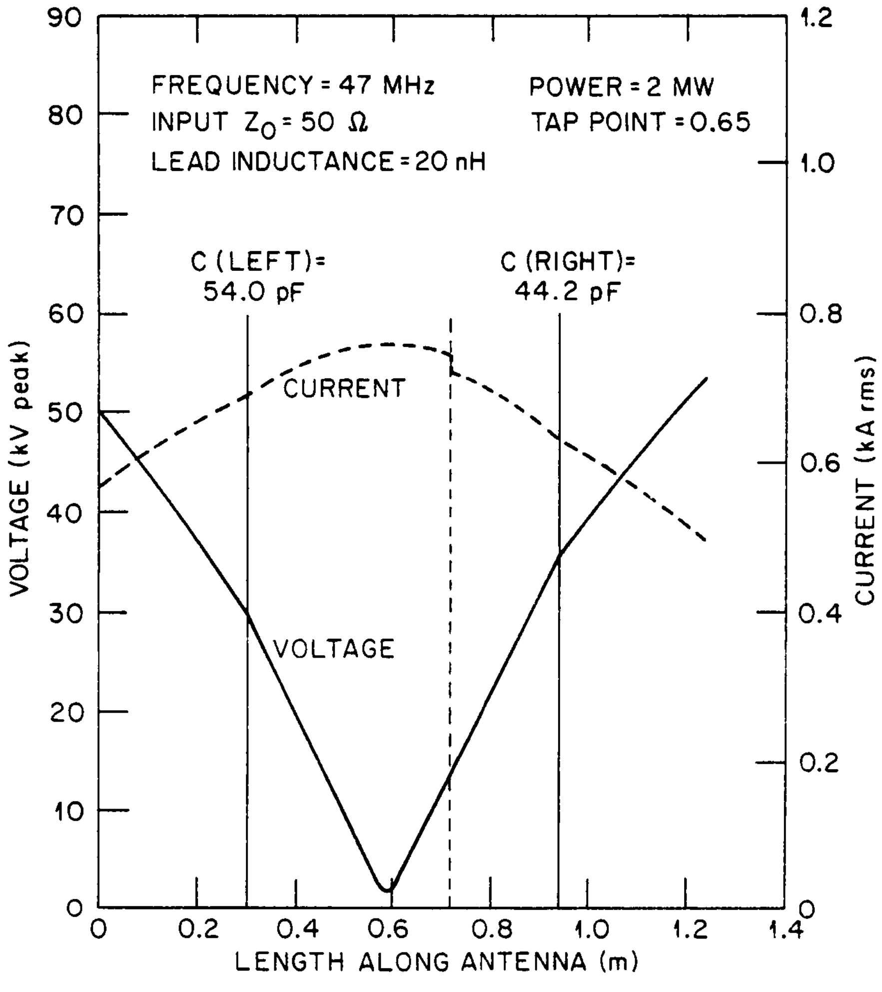

Fig. 9. ORNL RDL antenna voltage and current profiles.

CHAPTER III

MECHANICAL DESIGN SYNTHESIS

The mechanical objective of rf technology is the design and construction of an antenna that satisfies the electrical circuit constraints and functions reliably in the machine and plasma-imposed environment.

ORNL RDL Antenna Overview

The ORNL RDL antenna for TFTR is designed to launch fast waves from the low-magnetic-field side of the plasma. The target parameters are to deliver 4 MW of power to the plasma at a nominal initial frequency of 47 MHz. The antenna will operate in a pulsed mode for 2 s every 5 min and should be tunable from 40 to 80 MHz. Tuning can be made in two bands; the first band will be from approximately 40 to 60 MHz. In addition, the antenna can be tuned between machine pulses.

The antenna is required to fit into a horizontal midplane port that measures 23 in. wide by 35 in. high. It is capable of being remotely retracted 11 cm from a fully inserted position corresponding to 1 cm away from the plasma edge, which is defined as the last closed flux surface. Surfaces directly exposed to the plasma must consist of low-Z materials to minimize impurity contamination of the plasma. Since all components are in a high magnetic field, the antenna must be constructed of nonmagnetic material so as not to perturb the confining magnetic field and to minimize magnetic forces on components.

The antenna structure must be self-supporting off the port cover flange and be capable of withstanding the forces induced by the interaction of eddy currents produced when the poloidal magnetic field collapses during a disruption with the background magnetic field. The antenna Faraday shield must be capable of rejecting the heat input during a pulse from as much as 165 W/cm^2 of resistive rf power as well as a 100-W/cm^2 radial plasma flux and up to 2000 W/cm^2 toroidal plasma flux before the next pulse.

The ORNL RDL antenna, as installed on TFTR at a nominal operating position of 4 cm from the plasma edge, is shown in Figs. 10 and 11. The mechanical configuration consists of two asymmetric RDL circuits positioned side by side, each delivering 2 MW. The two current straps are enclosed in separate cavities by a single, water-cooled Faraday shield assembly containing a dividing wall. The front of the Faraday shield facing the plasma is graphite covered. Each of the current straps has two remotely adjustable vacuum capacitors. The 50-Ω impedance vacuum feedthrough feeding each current strap marks the interface point between

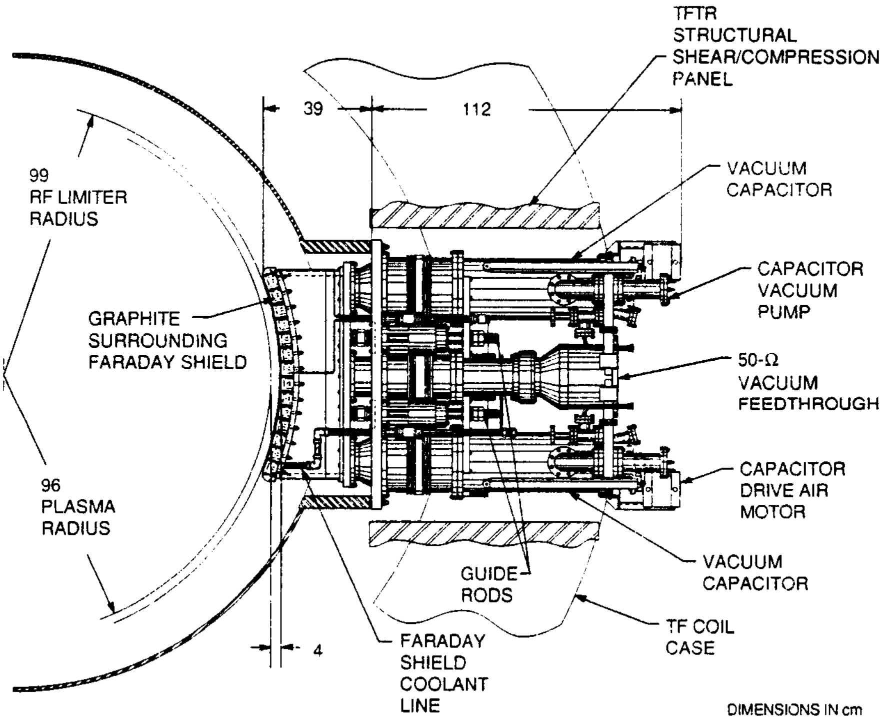

Fig. 10. ORNL RDL antenna installation elevation view.

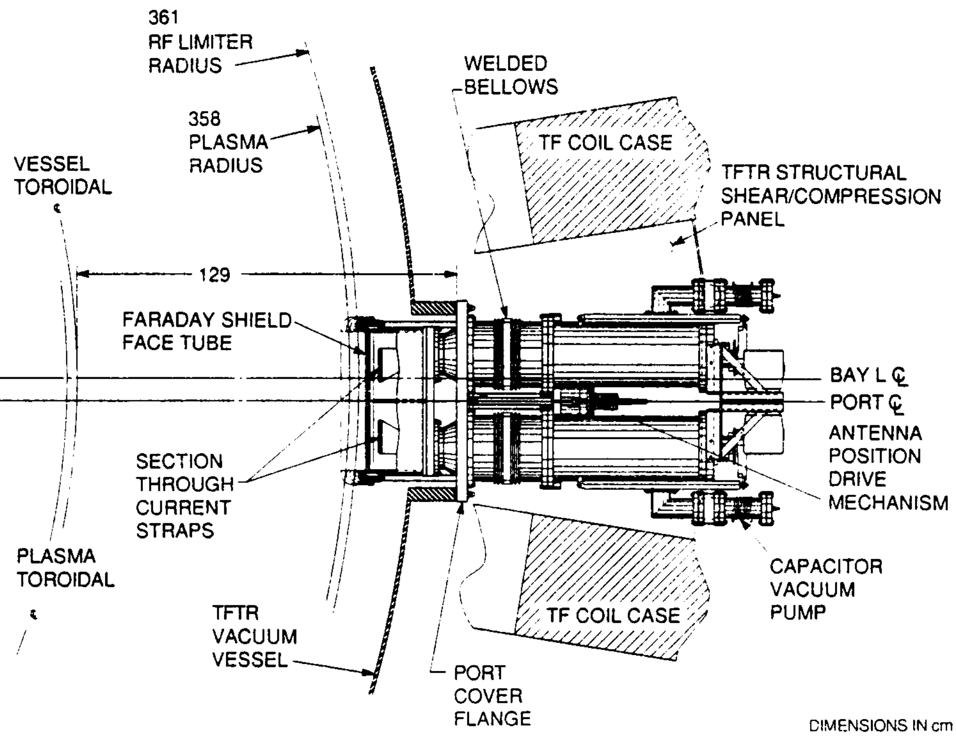

Fig. 11. ORNL RDL antenna installation plan view.

the antenna and the rest of the transmission system. The entire assembly is supported by four guide rods counteracting all forces to the port cover flange and is positioned by a single, centered drive mechanism. All penetrations of the vacuum vessel are bellows sealed. The major structural material is 304L stainless steel, and all rf conducting surfaces consist of copper plating on the stainless steel.

Global Parameters

Development of the basic configuration begins with certain global physical and electrical parameters that are essentially fixed at conception. Design considerations dictate that the antenna must fit through the port envelope and must not interfere with other machine hardware outside the port. Figure 11 shows the space limitations imposed by the TF coils, and Fig. 10 shows restrictions imposed by the shear/compression structural panels spanning the gap between TF coils above and below the port. Effectively, the antenna must fit into a cavern approximately 3 ft deep. Ease of installation is an important consideration. Figure 12 shows that most of the port cover flange bolts are shadowed by the final assembly. Access must be available for tightening the bolts. Consequently, the antenna design must accommodate removal of all structures interfering with installation of the bolts.

Maximum utilization of the available envelope inside the port is dictated primarily by electrical considerations. The poloidal length of the current strap is an important factor in determining power transmission in that it dictates the extent of the flux available for coupling to the plasma. The current strap must be long enough to allow sufficient flux linkage to transmit the required power. For the given envelope, the length of a current strap is sufficient to transmit only 2 MW. Consequently, two current straps must be positioned side by side in the port to transmit the required 4 MW. The necessity of two current straps immediately doubles the remaining circuitry hardware, namely, the capacitors and feedthroughs.

The toroidal width of the port dictates the maximum cavity width for each current strap. The current strap width itself is determined by the cavity dimension. Studies at ORNL indicate that, to minimize induction with the walls and to produce the optimum flux field, the current strap should occupy approximately 50% of the cavity width.[6] Initial investigations considered a single cavity with no dividing wall housing both current straps. This permitted flux linkage between straps and indicated difficulty in isolating control of individual straps. Consequently, a dividing wall was added to the design to isolate the two straps from each other.

---

[6] C. Rettig et al., "Measurements of the Loading Impedance and Field Scaling of a Cavity ICRF Launcher for Big D," *Bull. Am. Phys. Soc.* **30**(9), paper 8P14 (1985).

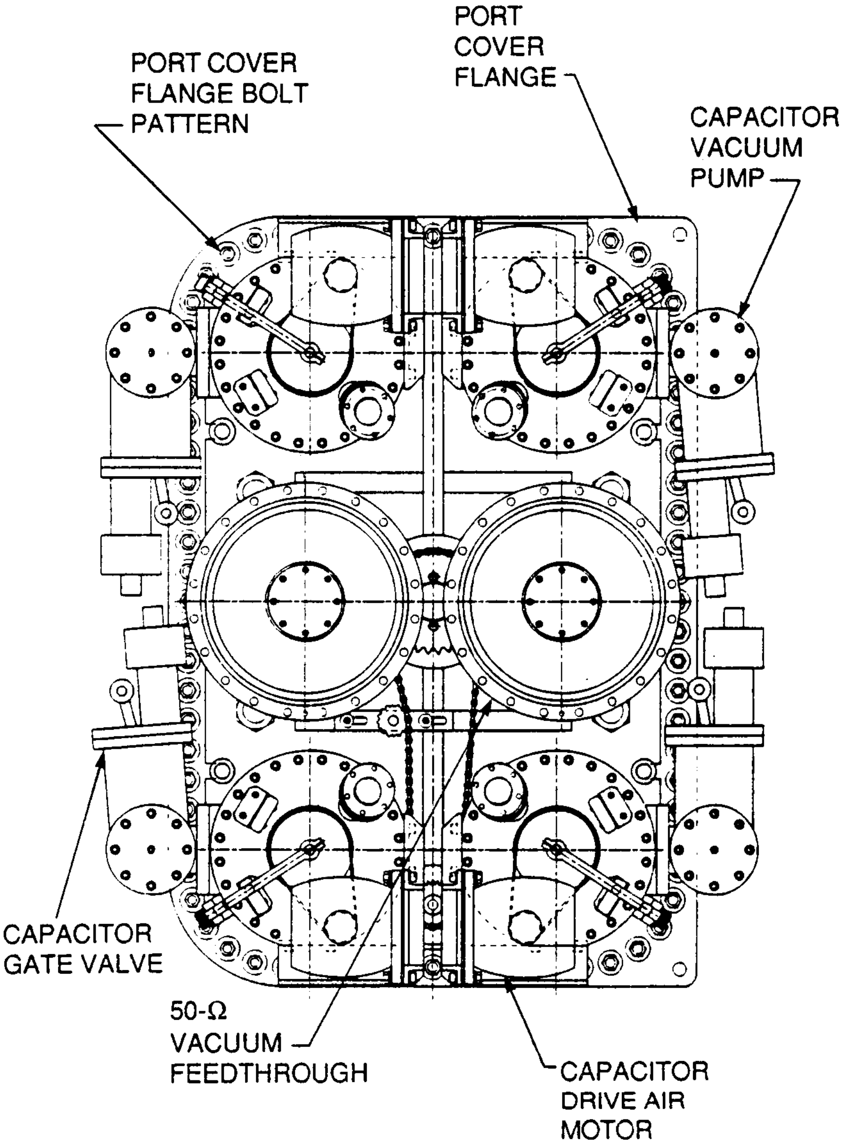

Fig. 12. ORNL RDL antenna installation end view.

The radial separation between the back edge of the current strap and the cavity back wall is another electrical parameter influencing the antenna configuration. Ideally, it is desirable to have all the energy in the flux around the current strap available for coupling to the plasma. Flux linkage to the side walls is unavoidable because of space restrictions. However, the back wall can be moved away so that no significant currents are induced and minimal power is lost in joule heating of the back wall. Studies at ORNL have shown that a back wall recess of $\geq$6 in. reduces these negative effects to negligible levels.

Flux linkage to the plasma is controlled by the proximity of the current strap to the plasma edge. Since the plasma has a toroidal geometry, the current strap must follow the poloidal curvature to maintain the spacing between the strap and the plasma. Although toroidal curvature is also desirable, the associated complications in the Faraday shield precluded curvature in this design.

When the global parameters have been satisfied, synthesis of the antenna electrical configuration is complete. The remainder of the design process concentrates on the specific issues surrounding electrical compatibility of the detail design and thermal and structural responses to the operating environment.

Detail design of the antenna can be divided in terms of specific subsystems. The heart of the electrical circuit is composed of the feedthrough, coaxial conductor, current strap, and capacitors. The mechanical backbone of the assembly is the support structure, which supports bulk movement and acquires positional stability from the main drive system. Finally, the Faraday shield controls wave polarization while being subjected to the harshest environment of all nonlimiter hardware penetrating the first wall of a tokamak.

Electrical Circuit Components

An assembly cross section through one of the two asymmetric RDL circuits is shown in Fig. 13. An isolated view clarifies the arrangement in Fig. 14. The input to the circuit is the rf vacuum feedthrough. The feedthrough is one of the crucial elements of the system in that it must handle high voltages and currents and serve as the barrier between the pressurized transmission line and the evacuated region of the antenna. Its failure not only affects the rf system but also means loss of vacuum and operation shutdown of the machine. Structural integrity of this element is essential. Historically, the feedthrough has often been the weak link in voltage handling of antenna circuitry. ORNL personnel have developed a feedthrough concept that increases both reliability and capability over contemporary hardware.[7] The feedthrough uses a cylindrical alumina ceramic vacuum barrier brazed between copper end caps. The end caps allow mechanical vacuum seals between tapered inner and outer coaxial conductors. The ceramic is much longer than its diameter, permitting the use of very gradual tapers on the coaxial conductors. This configuration produces an electric field that is nearly perpendicular to the ceramic surface along its length, which minimizes the possibility of surface breakdown. A constant characteristic impedance of 50 Ω is a requirement for matching to the 50-Ω input line and is made possible by the use of straight tapers on the inner and outer conductors. The approximate equation for the characteristic impedance (in ohms) at a cross section through the feedthrough is

$$Z_{\text{in}} = \frac{1}{2\pi} \sqrt{\frac{\mu_0}{\epsilon_0}} \ln \frac{b}{a} \,, \tag{55}$$

---

[7]T. L. Owens et al., "Radio Frequency Vacuum Feedthroughs for High-Power ICRF Heating Applications," *Fusion Technol.* (Proceedings of the 6th Topical Meeting on the Technology of Fusion Energy, San Francisco, Calif., March 1985) 8(1), 381 (1985).

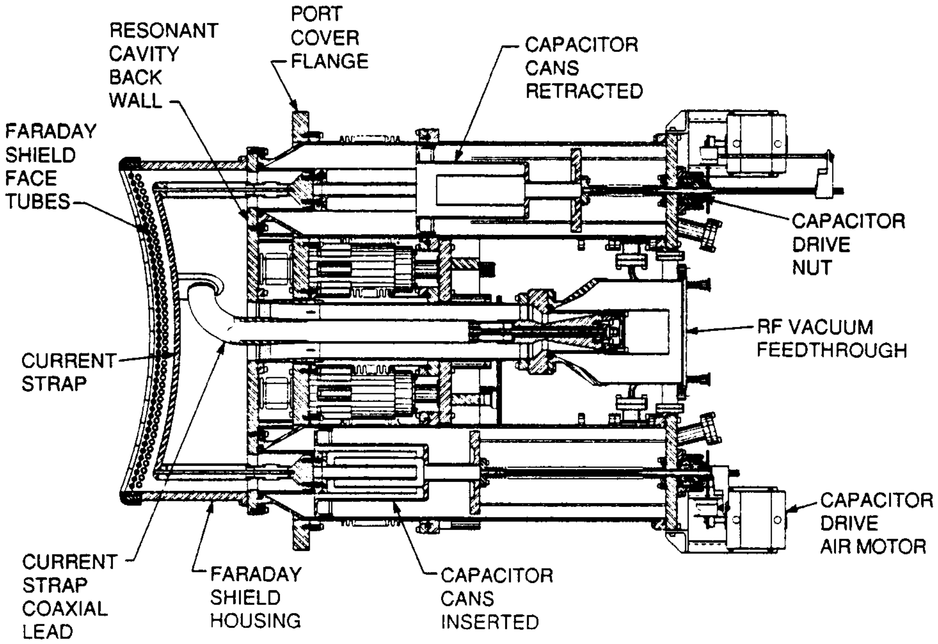

Fig. 13. ORNL RDL antenna current strap cross section.

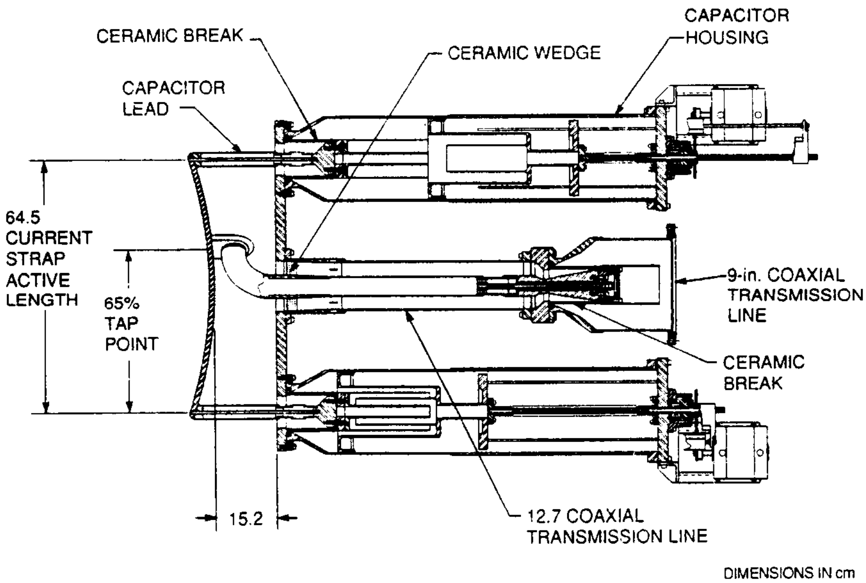

Fig. 14. ORNL RDL antenna circuit subassembly.

where

$$b = \text{outer conductor diameter,}$$

$$a = \text{inner conductor diameter,}$$

$$\mu_0 = 4\pi \times 10^{-7} \text{ H/m,}$$

$$\epsilon_0 = 8.854 \times 10^{-12} \text{ F/m.}$$

For 50 Ω, this equation reduces to

$$\frac{b}{a} = 2.302 \; . \tag{56}$$

The 50-Ω coaxial lead feeding the current strap is limited in size because of space restrictions. Consequently, the rf feedthrough must also serve as a reducer between a standard 9-in. coaxial transmission line to the antenna-specific 5-in. coaxial line. The antenna 50-Ω coaxial lead terminates at the back wall of the current strap cavity. Physical limitations force the coaxial lead to be on axis with the current strap centerline. Consequently, as the coaxial inner conductor passes through the cavity back wall, it must bend to reach the asymmetric feedpoint of the current strap. Once past the cavity back wall, the coaxial conductor no longer has a 50-Ω characteristic impedance. The length of this conductor adds a finite, but tolerable, lead inductance to the RDL circuit which is essentially fixed by the degree of asymmetry in the tap point plus the minimum spacing between the current strap and the back wall.

The basic geometry of the current strap has already been established by global parameters, resulting in a toroidal width of 4.50 in. (11.43 cm) and a vertical height of 26.38 in. (67.01 cm). A poloidal curvature of 41.58 in. (105.61 cm) increases the strap effective length to 26.84 in. (68.18 cm). The tap point is chosen to produce a match at the nominal 47-MHz operating frequency. Computational results set the point at 65% of the strap poloidal length.

Ideally, the two capacitors would connect directly to the ends of the current strap. Any additional noncoaxial conductor length, as with the 50-Ω coaxial lead, adds a certain amount of lead inductance to the circuit. The inductance of the strap lead, coupling primarily to the cavity top and bottom walls, can be minimized if the strap lead is wide in the toroidal direction. This has the effect of localizing most of the current, and hence the flux, on the edges of the lead instead of on the sides parallel to the cavity top and bottom walls. A circular configuration, however, is required to interface with the capacitor. Consequently, the strap lead has a tapered shape making the transition between the current strap width and the circular interface with the capacitor.

Commercially available vacuum variable capacitors exist which are capable of delivering most of the required capacitance range. They are probably adequate in standoff voltage rating. The real concern for their use in this application is the industry-rated maximum operating current, which is limited by cooling capacity before overheating occurs. The continuous-wave current rating of currently produced capacitors may be adequate for the antenna pulsed operation. However, schedule restrictions of the project prohibited verification of commercial capacitor overall performance, and the decision was made to design and fabricate custom capacitors for the antenna.

A variable capacitor consists of two sets of nontouching concentric cans. If one set is moved relative to the other, the areas of the overlapping surfaces are changed. This change in area thus varies the extent of the electric field between surfaces and hence the magnitude of stored electric energy.

The capacitor is a very high voltage element in the circuit (50 to 70 kV). Although the tokamak is essentially a vacuum chamber, the presence of a plasma limits the vacuum attainable in the vicinity of the antenna to about 10^{-5} torr.

The vacuum region separating the cans of the capacitor needs to be in the 10^{-10}-torr range for maximum voltage handling. Consequently, the capacitor design, as shown in Fig. 15, incorporates a ceramic break separating the capacitor vacuum from the machine vacuum. The cylindrical ceramic break is the same design used in the 50-Ω feedthrough. The capacitor vacuum is maintained by a rechargeable, zirconium-aluminum getter vacuum pump. The nonmagnetic construction of the pump permits its location adjacent to the capacitor vacuum chamber, which enhances ultimate pumping speed. The vacuum pumping system also incorporates a gate valve, specifically for isolating the pump getter surfaces from atmospheric saturation during disassembly and removal once the pump has been activated.

The fixed set of capacitor cans interfaces with the current strap lead at the unsupported end of the ceramic cylinder. The variable set of capacitor cans makes electrical contact with the housing ground plane through sliding finger stock around the outer edge. The variable cans are moved linearly by an adjustable, nonmagnetic air motor driving a novel, helical-pitch ball nut and "threadless" screw device. The lack of threads on the drive rod facilitates use of the long, thin welded bellows, and the need for a sliding air-to-vacuum interface is thus eliminated.

The inability to short the current strap circuit to the housing ground plane poses special problems for mechanical support during thermal excursions and disruption loading events. A summary of the current strap forces is shown in Fig. 16.

Joule heating of the current strap during a 2-s pulse with as much as 100 W/cm^2 heat input will result in bulk thermal expansion of the strap. Ultimate expansion of the current strap is limited by the equilibrium temperature reached between the cyclic heat input and radiative cooling between pulses. The differential expansion between the current strap and the cavity back wall where the capacitors are affixed will result in a bending moment transmitted through

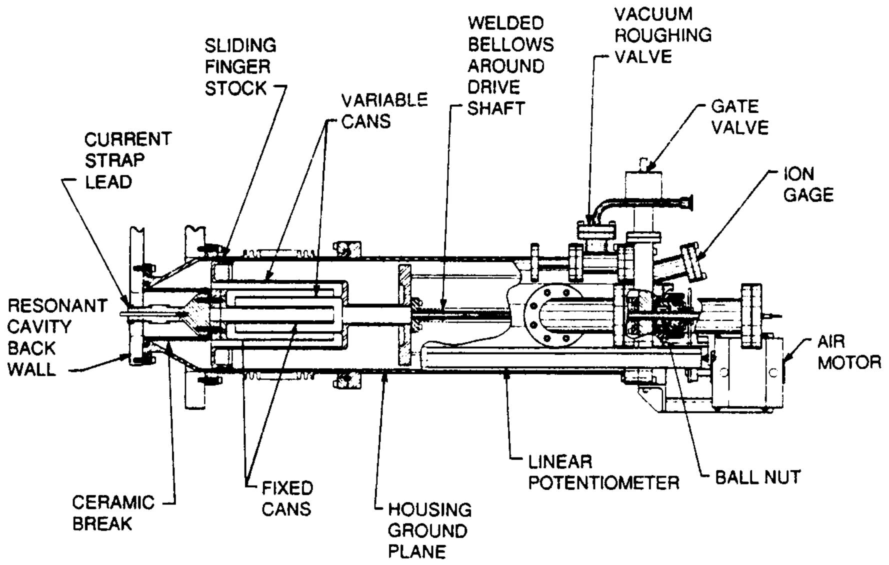

Fig. 15. ORNL RDL antenna capacitor subassembly.

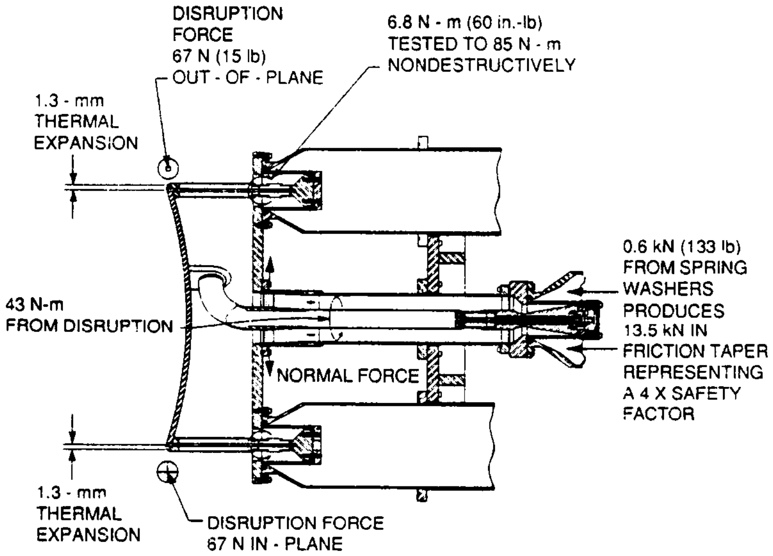

Fig. 16. ORNL RDL antenna current strap forces.

the strap lead to the capacitor ceramic break. Since alumina ceramic is weak in bending or tension, minimizing this bending moment is essential. The resulting design minimizes the rigidity of the interface of the strap lead to the ceramic by passing a slender rod through the hollow lead. Vertical deflection of the lead relative to the ceramic is accommodated by incorporating a formed bellows as part of the lead conducting surface. The relatively small, lateral spring constant of the bellows and the low moment of inertia of the rod limit the moment transferred to the ceramic to values much less than the ceramic has survived in nondestructive testing.

A disruption event occurs when the plasma becomes unstable and rapidly expands to the vacuum vessel wall in the time scale of milliseconds. When this occurs, the toroidal plasma current, which has been producing the confining poloidal magnetic field, collapses, and this results in collapse in the poloidal field. As the poloidal field collapses through any structure providing a complete conducting circuit oriented orthogonal to the collapsing field, it will induce eddy currents according to

$$I = \frac{\dot{B} A_s A_x}{\rho} , \tag{57}$$

where

I = eddy current (A),

$\dot{B}$ = flux collapse (T/s),

A_s = area of circuit through which $\dot{B}$ acts (m^2),

A_x = cross-sectional area conducting structure (m^2),

ρ = resistivity of conducting structure ($\Omega \cdot m$).

The induced current, in turn, interacts with the background vertical field to produce distributed forces on the conducting members according to

$$F = B_v I \ , \tag{58}$$

where F represents the forces (N/m) and B_v is the background field (T).

Depending on the resistivity of the structure, large forces may be developed. Although a disruption occurs over a time scale of 3 to 5 ms, the natural frequency of most stiff structures is sufficiently low to force treatment of the disruption forces as steady-state loads as far as mechanical stress analysis is concerned.

Since this project is performed in conjunction with PPPL, investigators at PPPL evaluated and supplied ORNL with the input force values on the structure. Consequently, mechanical design was limited to evaluation of the effects of these input forces.

Disruption events will produce opposing forces acting on each end of the current strap, as shown in Fig. 16, tending to twist the strap about the center coaxial conductor axis like a propeller. To resist this torque, a ceramic wedge is placed in the coaxial line annulus as shown in Fig. 17. The ceramic is machined with a self-holding friction taper on both inside and outside diameters. Corresponding tapers exist on the inner and outer conductors. The frictional force developed on the tapered surfaces counteracts the torque produced during a disruption. The wedge surface normal force required to maintain the friction is produced by pulling the coaxial center conductor toward the 50-Ω feedthrough. The axial freedom required for this operation is afforded by a plug-and-socket joint between the feedthrough and the coaxial conductor center. The center conductor has a threaded rod extending through the feedthrough to the far side of the feedthrough ceramic. Tightening a pair of nuts in the feedthrough puts the coaxial center conductor in tension and produces the required friction on the ceramic wedge. This arrangement has the benefit of applying only a compressive load on the feedthrough ceramic, which it

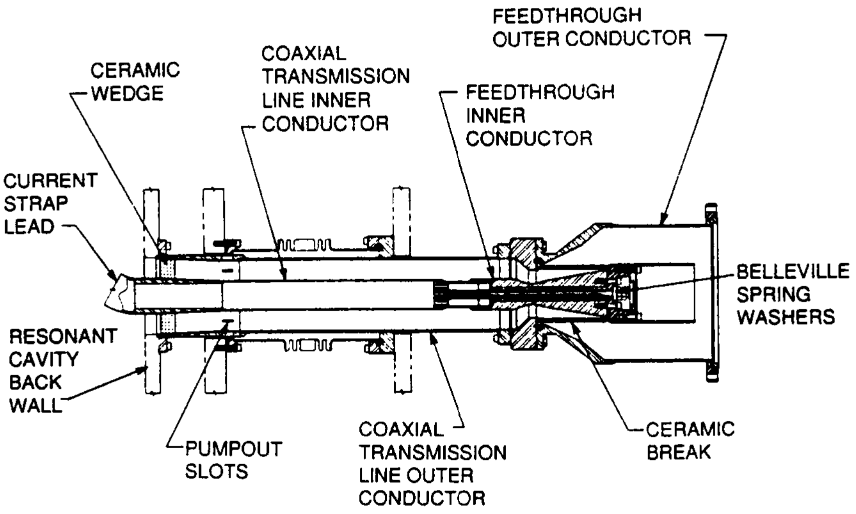

Fig. 17. ORNL RDL antenna coaxial/feedthrough subassembly.

can handle easily. The friction force is maintained during thermal expansion by the use of Belleville spring washers under the two retaining nuts in the feedthrough.

Support Structure

The cavity back wall has already played a key role in determining stresses due to thermal expansion imparted to the capacitor ceramics. The back wall, as shown in Fig. 18, is an integral part of the antenna support structure.

The support structure consists of four 1.50-in.-diam Inconel-718 guide rods welded to the cavity back wall and extending through clearance holes in the port cover flange to threaded connections at the assembly tie-down plate. The guide rods transfer all forces through Vespel bushings retained in housings that are fixed to the port cover flange. The length of each guide rod that extends into the vacuum is enclosed in a welded bellows. The bellows allow all bushings to remain in air, eliminating unwanted outgassing from the bushing and surface galling in a vacuum. The tie-down plate is the mechanical counterpart of the cavity back wall

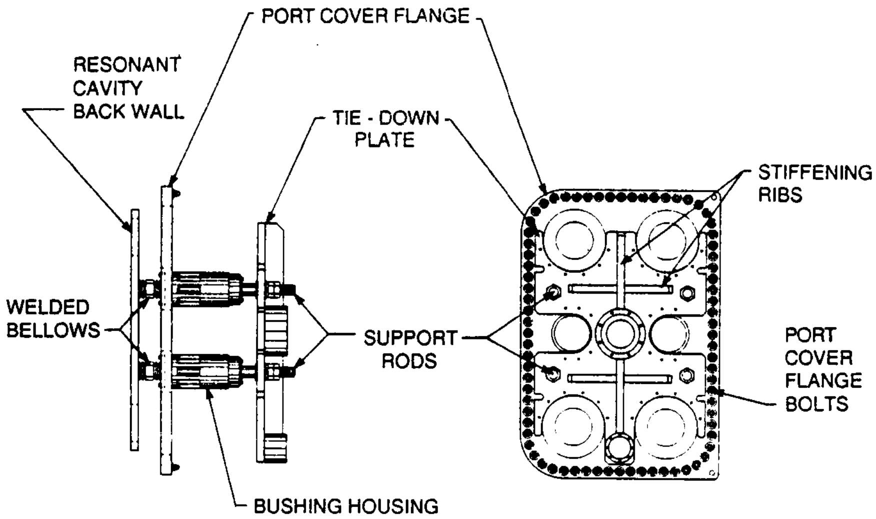

Fig. 18. ORNL RDL antenna support structure subassembly.

on the outside of the port cover flange. It is equipped with stiffeners to reduce deflection of the plate due to the atmospheric pressure on the six welded bellows enclosing each tube extension through the port. The tie-down plate also represents the interface between the support and drive systems.

The use of high-strength Inconel-718 guide rods is a conservative measure to counteract the high disruption forces on the structure. Analysis by PPPL concludes that as much as 11,630 lb of transverse force can be imparted to the end of a rod during a severe disruption. If the antenna is at one end of its stroke when this occurs, the cantilever loading of a rod results in a bending stress of 105,200 psi, which is 59% of the yield strength of the material.

Drive System

The drive system interfaces with the structural tie-down plate by moving it, and consequently the entire assembly, back and forth. An installation cross section through the drive system is shown in Fig. 19, and an isolated view of the system clarifies the arrangement in Fig. 20.

The primary load the system must counteract is caused by atmospheric pressure on the six tube extension bellows. The bellows have a combined force of 4970 lb always directed toward the port cover flange. The system contains a single drive point, which increases reliability by eliminating the problems encountered with synchronization and alignment of multiple drive points. The main problem, finding a threaded system strong enough to handle the forces while retaining sensitivity of adjustment, was solved by using a buttress thread system. The buttress thread form works well in either a pushing mode or a pulling mode, but not both. This application is adequate since the vacuum load always pushes in the same direction. An aluminum bronze drive nut is used to reduce friction and galling. The drive nut is supported by self-aligning roller thrust bearings. The system is designed in excess of the vacuum requirements since radial forces due to disruptions will also be encountered.

One stipulation imposed by PPPL was for the interface at the drive system input to remain stationary and not track with the antenna assembly during positioning. Consequently, the design incorporates a ball spline in which the spline shaft rotates in a stationary position, transferring torque through a nut that tracks along the shaft. A sprocket-and-chain assembly transfers the input torque from the spline nut to the aluminum bronze drive nut.

Faraday Shield

The Faraday shield, with its close proximity to the plasma and the current strap, is the antenna component that experiences the harshest operating environment. Electrical and mechanical reliability of the antenna rests heavily on the

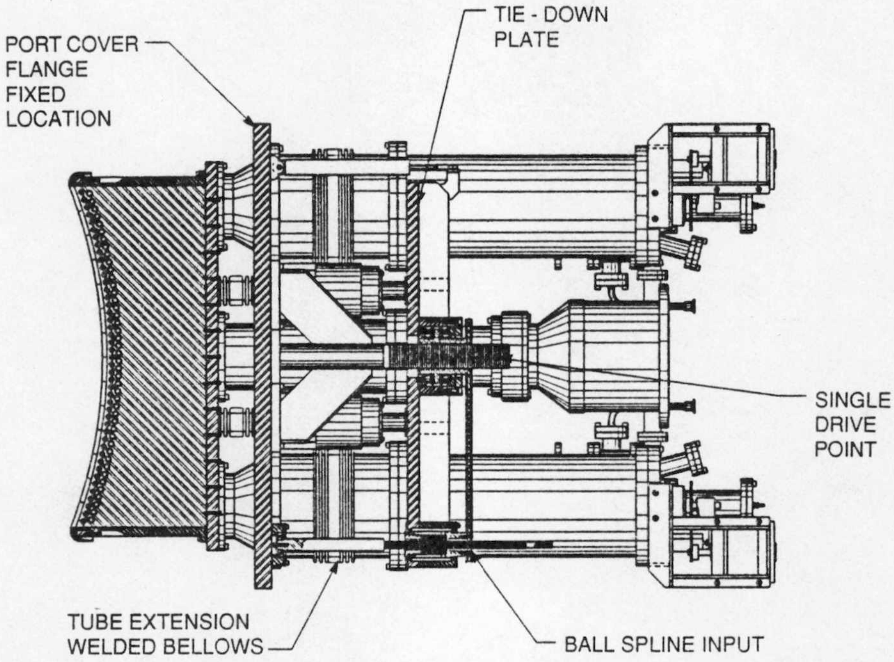

Fig. 19. ORNL RDL antenna main drive cross section.

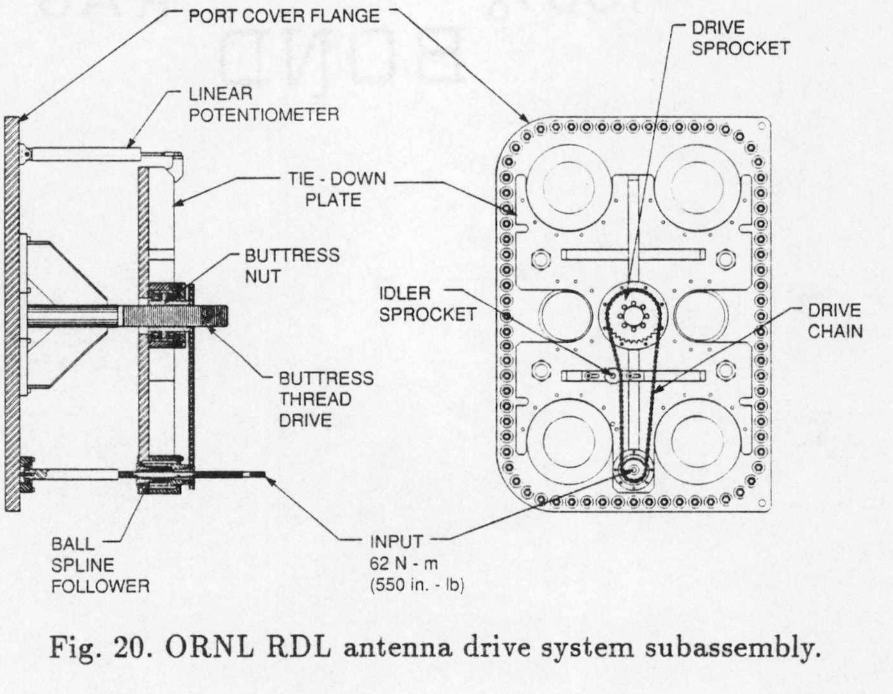

Fig. 20. ORNL RDL antenna drive system subassembly.

adequacy of the shield design. ORNL personnel have investigated numerous Faraday shield configurations in an effort to improve the electrical performance and mechanical capabilities needed for increasingly harsh plasma environments and power requirements.[8]

While the primary rf functions of the Faraday shield are to transmit the desired wave component and polarization, it must have sufficient optical opacity to protect the internal antenna elements from the plasma. The shield must have circuit characteristics that minimize voltages and electric fields and maximize power through the system. Mechanically, the shield must be able to withstand high plasma particle and heat fluxes, as well as disruption-induced forces.

The Faraday shield configuration for launching fast waves is essentially a set of toroidally oriented conducting elements. Researchers at ORNL measured rf transmission and shaping of the flux field as a function of element shape and spacing. Mechanical considerations of fabricability and cooling, as well as plasma consideration of impurity reduction, were influences in the element shapes that were tested. The ORNL study concluded that a two-tier array of tubing with a nominal 0.125-in. (3.18-mm) gap separating the tubes was the most attractive configuration, allowing approximately 85% flux transmission while offering good fabrication and cooling capabilities.

The Faraday shield for the ORNL RDL antenna is integral with the side walls forming the cavities around the current straps. This configuration facilitates fabrication and handling at final assembly. The specific relationship between the side walls and the current straps was discussed under the section Global Parameters.

---

[8] D. J. Hoffman et al., "Material and Electromagnetic Properties of Faraday Shields for Ion Cyclotron Heating Antennas," *Fusion Technol.* (Proceedings of the 6th Topical Meeting on the Technology of Fusion Energy, San Francisco, Calif., March 1985) 8(1), 392 (1985).

One further relationship studied at ORNL was the proximity of the Faraday shield to the current straps. For optimum wave transmission, the spacing between the back edge of the Faraday shield elements and the current strap is 0.59 in. (1.5 cm).

The specific design of the Faraday shield, as shown in Figs. 21 and 22, includes two-tier, straight, Inconel-625 tubes with semicylindrical graphite segments brazed to the front row facing the plasma only. Full-length side manifolds form a single-pass, reverse-flow cooling circuit. The front and sides of the manifolds are protected by thick, modular, passively cooled graphite bumpers.

The front-row tubes are nominally 0.375 in. (9.53 mm) in outside diameter and 0.065 in. (1.65 mm) in wall thickness. The semicylindrical graphite segments are 0.062 in. (1.57 mm) thick, forming an effective tube profile diameter of 0.50 in. (12.70 mm). The back-row tubes are 0.50 in. (12.70 mm) in outside diameter and 0.065 in. (1.65 mm) in wall thickness. Brazing of the graphite segments to the front tubes required some development. The tubes were first copper-plated for electrical conduction. The graphite was brazed as 1.00-in.-long (25.4-mm) segments having angled ends overlapping each other. Ticusil brazing alloy was used, chosen specifically for its high remelt temperature of approximately 760°C. The alloy was chosen to be 0.002 in. (0.05 mm) thick to minimize the wicking action into the expansion joints between the graphite segments.

The cooling system uses an all-welded construction to maximize reliability for in-vacuum use. The tubes are welded to and integral with the cavity side walls. Subsequently, the manifolds are welded to the side walls, forming the coolant passages. Each tube is tack-welded to the cavity center wall for good electrical contact and mechanical strength.

During a 2-s pulse, the Faraday shield tubes are exposed to as much as 100 W/cm^2 plasma radial heat flux and 165 W/cm^2 rf-deposited heat flux. The

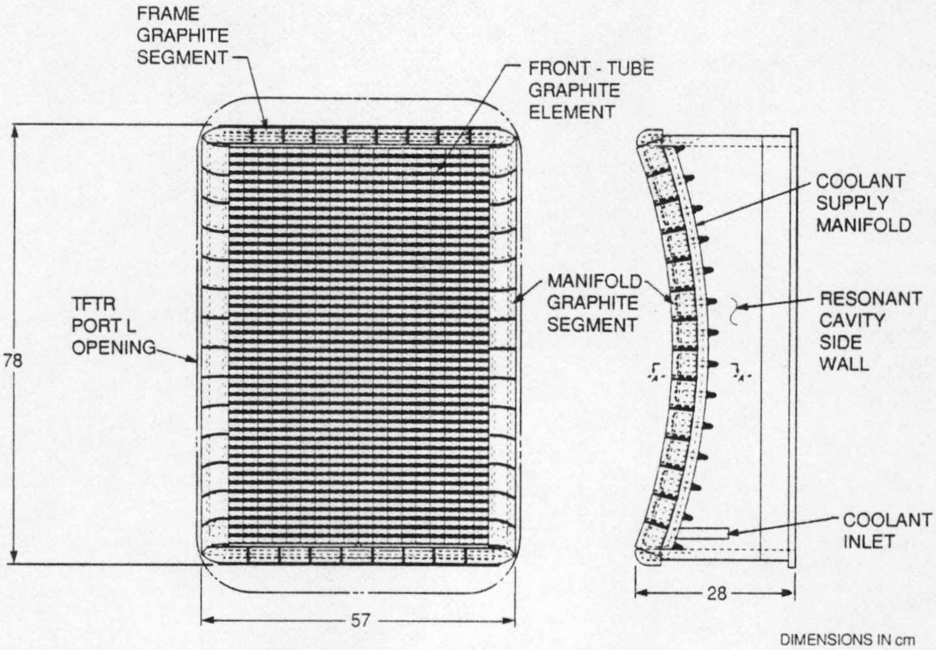

Fig. 21. ORNL RDL antenna Faraday shield subassembly.

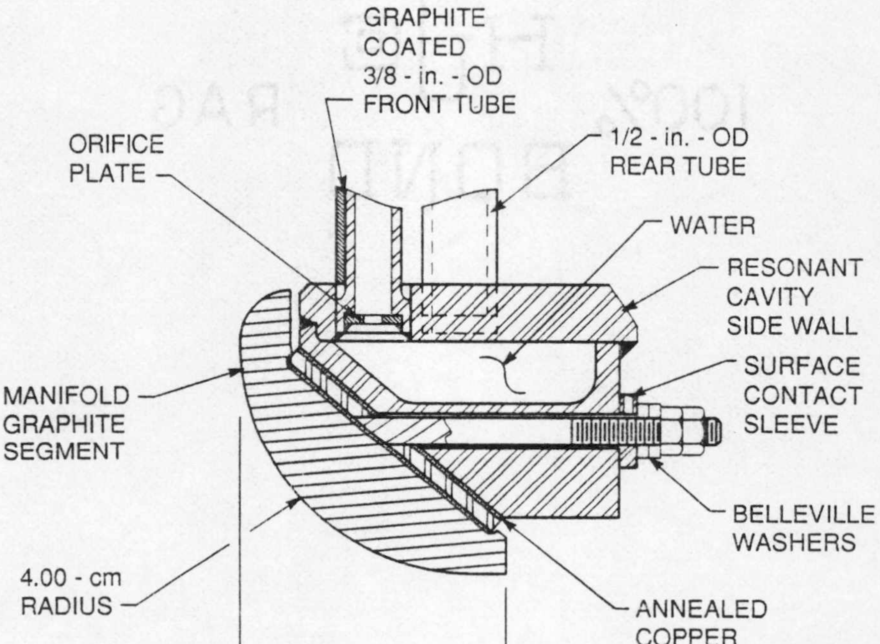

Fig. 22. ORNL RDL antenna Faraday shield manifold cross section.

presence of the electrically resistive graphite on the front tubes means that about 55 to 60% of the rf heat flux shows up as joule heating on the same side of the front tubes as the impinging plasma radial heat flux. The rear tubes see only the plasma radial flux that passes through the gap between front-row tubes. The result of the uneven heat flux between front and rear tubes is that the front tubes require more cooling water than the rear tubes. Both rows of tubes are fed from a common manifold, and this arrangement is complicated by the fact that the manifold is supplied at one end. Therefore, a thorough hydraulic analysis was performed to determine orifice sizing and coolant distribution from front to rear tubes and along the length of the manifold. For a 38-gpm total flow rate, divided as 24 gpm for all the front tubes and 14 gpm for all the rear tubes, the maximum calculated graphite temperature is approximately 260°C.

The maximum stress on a Faraday shield tube is a result of thermally and mechanically induced stresses. Since thermal expansion of a tube is restrained, bulk thermal expansion will produce compressive stresses. At a cross section, as the temperature of the side of a tube facing the plasma exceeds the temperature of the side of the tube away from the plasma, bending stresses are produced. There is a hoop stress produced by the internal coolant pressure. The remaining two stresses are induced by a disruption. The eddy current induced in a tube, as determined by PPPL, produces a line load along the tube of 2.60 lb/in., which produces a bending stress. During a disruption, the cavity walls try to move relative to each other, producing another bending stress in the tube. A summary of the "worst-case" tube stresses is presented in Table 1.

A superposition of all the load cases results in a maximum fiber stress of 30,170 psi in a tube. An engineering estimate of the fatigue life of Inconel-625, under the conservative assumption of maximum thermal and disruptive loadings on every pulse of the machine, results in an estimated fatigue life in excess of 10^5 cycles, which is adequate for the projected life of this experiment on TFTR.

Table 1

Tube stresses produced by worst-case thermal and mechanical excursions

Inducing mechanism	Stress (psi)
Restrained thermal growth (compression)	9,951
Temperature gradient across tube (bending)	14,335
Internal pressure (bending)	490
Disruptive line load (bending)	4,389
Frame deflection (bending)	6,292

CHAPTER IV

FUTURE DESIGN CONSIDERATIONS

Ion cyclotron resonant heating is perceived as the mechanism for raising the temperature of ohmically heated reactor plasmas to ignition temperatures. Demonstrating the power delivery capabilities of specific ICRF antenna concepts is the present goal. Extrapolation of present antenna technology to reactor applications must accompany the technological development of future fusion experiments. The ORNL RDL antenna represents the first significant step in the evolution of compact loop ICRF antennas. It will demonstrate the compact loop concept and the adequacy of the design of the basic circuitry configuration. Although TFTR imposes a mechanically demanding operating environment, future antenna design will involve much development to fulfill the requirements of a power-producing fusion reactor. Design principals of the ORNL RDL antenna will serve as building blocks toward the realization of ICRF antennas as the dominant supplemental plasma heating devices.

Aspects of reactor design that will impose new and more stringent requirements of antenna design include minimizing the machine aspect ratio and magnetic field ripple, incorporation of a tritium breeding blanket and radiation shield, production of neutrons, increased pulse lengths, and increased plasma current.

Reducing the machine aspect ratio is an economical measure to reduce the size of the vacuum vessel. Reducing the size of the vessel imposes size restrictions on the antenna since port size will necessarily be minimized. Small ports are especially restrictive to the requirements of the resonant double loop concept. In conjunction with reducing the aspect ratio, minimizing the magnetic field ripple is important to plasma confinement. Ripple is decreased by increasing the number of toroidal field coils. This results in less space between adjacent coils and, once again, the reduction in port size. Contemporary reactor concepts have reduced the toroidal width of a port to the point that two current straps per port are required to be configured one on top of the other instead of side by side.

The introduction of a tritium breeding blanket and radiation shield around the machine increases the distance between the first wall penetration and the point where the antenna must interface with the transmission system. An increase in radial length increases the portion of the antenna structure that is subjected to the collapsing poloidal field in a disruption. An increase in structure length translates into increased forces.

Once ignition is achieved in a fusion machine, a substantial number of neutrons will be produced. Consequently, the antenna will become activated and the maintenance of the antenna becomes difficult. Antenna reliability becomes of paramount importance. However, it is inevitable that maintenance will have to be performed. Consequently, as with every system on a reactor, the antenna module must be compatible with remote-handling equipment. Interfacing the antenna with the remote-handling facilities will become a major design problem in the future.

A reactor will have to obtain an extended pulse length to be attractive as a commercial utility. An increased pulse length pushes the heat flux on the antenna into the steady-state regime. Relying on the heat capacity of the antenna structure with trace cooling between pulses will have to be replaced by active cooling on essentially every component of the circuitry and Faraday shield. Introducing cooling lines that do not ground the inner conductor of a coaxial arrangement is not a straightforward task. The addition of adequate cooling will be one of the most difficult design problems of future antennas.

Increased plasma current will inevitably accompany more powerful machines. Increasing the current will increase the disruption forces experienced by the antenna structure by as much as a factor of 30 over contemporary machines. Antennas cannot be designed to withstand such forces. The solution to the problem will be to eliminate the eddy currents in the structure by introducing electrical breaks into potentially destructive current loops.

In summary, future antennas will be required to handle higher heat fluxes, increased power densities, and larger disruption forces in a more geometrically restrictive envelope. At the same time, they must have maximum reliability and simplified remote-maintenance capabilities. The technology developed for compact loop ICRH antennas will provide the foundations for extrapolating to designs of other rf plasma heating and control devices.

BIBLIOGRAPHY

BIBLIOGRAPHY

Evrard, M. P., V. P. Bhatnagar, M. Bures, and F. Sand, "Comparison of Theoretical and Experimental ICRF Antenna-Plasma Coupling Resistance in JET," p. 133 in *Proceedings of 13th European Conference on Controlled Fusion and Plasma Heating, Schliersee, April 1986*, Contributed Papers, Part 2, European Physical Society, Schliersee, Germany, 1986.

Hoffman, D. J., F. W. Baity, W. R. Becraft, J. B. O. Caughman, and T. L. Owens, "Experimental Measurements of the Ion Cyclotron Antennas' Coupling and RF Characteristics," *Fusion Technol.* (Proceedings of the 6th Topical Meeting on the Technology of Fusion Energy, San Francisco, Calif., March 1985) **8**(1), 411 (1985).

Hoffman, D. J., F. W. Baity, W. E. Bryan, G. L. Chen, K. H. Luk, T. L. Owens, J. M. Ray, P. M. Ryan, D. W. Swain, and J. C. Walls, "The Design of High-Power ICRF Antennas for TFTR and Tore Supra," to be published in the Proceedings of the 7th Topical Conference on Applications of Radio-Frequency Power to Plasmas, Kissimmee, Fla., May 1987.

Hoffman, D. J., W. R. Becraft, F. W. Baity, J. B. O. Caughman, and C. C. Tsai, "Material and Electromagnetic Properties of Faraday Shields for Ion Cyclotron Heating Antennas," *Fusion Technol.* (Proceedings of the 6th Topical Meeting on the Technology of Fusion Energy, San Francisco, Calif., March 1985) **8**(1), 392 (1985).

Owens, T. L., F. W. Baity, D. J. Hoffman, and J. H. Whealton, "Radio Frequency Vacuum Feedthroughs for High-Power ICRF Heating Applications," in *Fusion Technol.* (Proceedings of the 6th Topical Meeting on the Technology of Fusion Energy, San Francisco, Calif., March 1985) **8**(1), 381 (1985).

Rettig, C., P. M. Ryan, and D. J. Hoffman, "Measurements of the Loading Impedance and Field Scaling of a Cavity ICRF Launcher for Big D," *Bull. Am. Phys. Soc.*, **30**(9), paper 8P14 (1985).

Uckan, N. A., class notes on fusion physics, engineering, and technology, The Univerity of Tennessee, Knoxville.

Weynants, R. R., D. Van Eester, V. P. Bhatnagar, and R. Koch, "Power Deposition Profiles in Textor Under ICRH Mode Conversion Conditions," p. 33 in *Proceedings of 13th European Conference on Controlled Fusion and Plasma Heating, Schliersee, April 1986*, Contributed Papers, Part 2, European Physical Society, Schliersee, Germany, 1986.

VITA

Wesley Emmett Bryan was born in Charlotte, North Carolina, on December 13, 1957. He entered the Co-Op program at the Georgia Institute of Technology in July 1976, and in June 1981 he received a Bachelor of Mechanical Engineering degree.

In July 1981, he accepted a position as staff engineer in the General Mechanical Engineering Department of Martin Marietta Energy Systems, Inc., in Oak Ridge, Tennessee. He was and currently is assigned to mechanical design in support of the Fusion Energy Division of the Oak Ridge National Laboratory.

He entered the Graduate School of The University of Tennessee, Knoxville, in September 1981 as a part-time student. He married Catherine G. Burns in January 1982.

He is a member of Lambda Chi Alpha, the Briaerean Society, and the American Society of Mechanical Engineers.